IEEE Access
Multidisciplinary | Rapid Review | Open Access Journal

Received August 1, 2019, accepted August 13, 2019, date of publication August 16, 2019, date of current version August 30, 2019.

Digital Object Identifier 10.1109/ACCESS.2019.2935806

Modeling and Stability Analysis of *LCL*-Type Grid-Connected Inverters: A Comprehensive Overview

YANG HAN[1], (Senior Member, IEEE), MENGLING YANG[1], HONG LI[2], PING YANG[1], LIN XU[3], ERNANE ANTÔNIO ALVES COELHO[4], AND JOSEP M. GUERRERO[5], (Fellow, IEEE)

[1]School of Mechanical and Electrical Engineering, University of Electronic Science and Technology of China, Chengdu 611731, China
[2]Aviation Industry Corporation of China, Chengdu Aircraft Industrial Corporation, Chengdu 610092, China
[3]Sichuan Electric Power Research Institute, Sichuan Electric Power Company, Chengdu 610072, China
[4]Faculty of Electrical Engineering, Universidade Federal de Uberlandia, Uberlandia 38400-902, Brazil
[5]Department of Energy Technology, Aalborg University, 9220 Aalborg, Denmark

Corresponding author: Yang Han (hanyang@uestc.edu.cn)

This work was supported in part by the Sichuan Province Key Research and Development Project under Grant 2017GZ0347, in part by the Natural Science Foundation of Guangdong Province under Grant 2018A030313494, and in part by the State Key Laboratory of Alternate Electrical Power System with Renewable Energy Sources under Grant LAPS18007.

ABSTRACT Due to the advantages of superior harmonics attenuation ability and reduced size, the *LCL* filter has been widely adopted to interface between the inverter and the grid for improving the quality of injected grid currents. However, the high-order characteristics and various constraints of the *LCL* filter complicate the filter design. Moreover, the stability of the internal current control loop of the individual inverter is susceptible to the inherent *LCL* -filter resonance peak. Meanwhile, the overall system stability would be aggravated by the external interactions between the inverter and the weak grid as well as among the paralleled inverters. Both the *LCL* -filter resonance peak and two types of interaction would cause severely distorted grid currents. Motivated by the existing problems, a comprehensive review on the modeling and stability analysis of the *LCL* -type grid-connected inverters is conducted in this paper. Concretely, the generalized parameter constraints of the *LCL* filter are outlined to facilitate the passive components selection, and the magnetic integration techniques of filter inductors are also introduced to reduce the weight and size of filter for increasing the power density of the system. Then, the various damping methods for enhancing the individual internal stability and the relevant application issues are also discussed. Furthermore, the impedance-based method for evaluating the system-level interactive stability is subsequently reviewed, with the emphasis on different modeling methods of inverter output impedance and online impedance measurement techniques. Finally, the future research trends on the modeling and stability analysis of *LCL* -type grid-connected inverters are also presented.

INDEX TERMS LCL-filter, grid-connected inverters, parameters design, magnetic integration, damping methods, delay, stability, impedance-based stability analysis, impedance modeling, impedance measurement.

I. INTRODUCTION

Recently, the distributed power generation systems (DPGS), as shown in Fig. 1, have been widely utilized for renewable energy integration, such as solar, wind, and fuel cell, which greatly alleviate the energy crisis and environmental problems [1]–[5]. Grid-connected inverters controlled by pulse-width modulation (PWM) techniques play the key roles for promoting the renewable energy consumption. However, the harmonics caused by PWM process would impose additional challenges on the conventional grid, such as the grid oscillation or even destabilization induced by distorted grid current. The passive filters are usually connected between the grid and the inverters to attenuate the high-frequency harmonics to improve the quality of injected grid current [6], [7].

In comparison, *L* filters are not suggested due to their poor high-frequency attenuation ability of −20 dB/dec and bulky inductors [8], yet *LC* filters are advantageous over *L* filters,

The associate editor coordinating the review of this article and approving it for publication was Madhav Manjrekar.

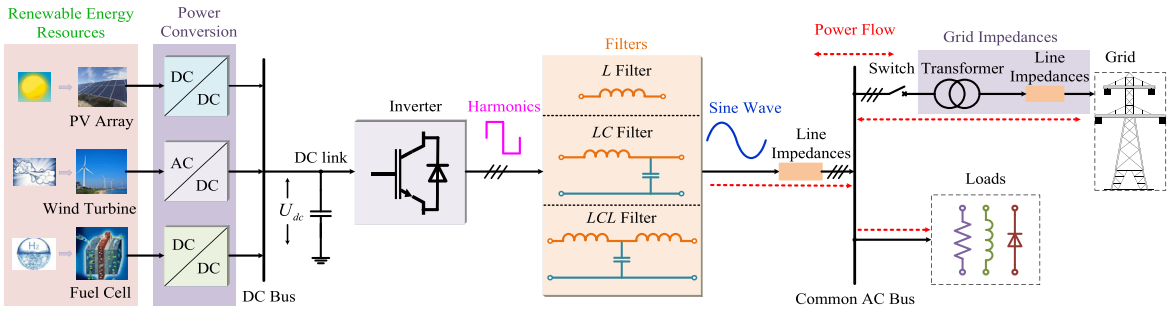

FIGURE 1. DPGS with the grid-connected inverter.

with the harmonics attenuation rate of −40 dB/dec [9], [10]. Nevertheless, compared with *L* and *LC* filters, the relatively small inductors and capacitors are required in *LCL* filters, and the superior high-frequency attenuation characteristic of −60 dB/dec can also be achieved simultaneously. In this scenario, *LCL*-type grid-connected inverters are preferred to be adopted on a large scale in practical applications [11]–[17].

It is worth noting that, the filtering performance of *LCL*-filter can be maximized by means of reasonable filter design, thereby avoiding the undesired stability problems resulting from the harmonics pollution to great extent. Nonetheless, the high-order *LCL* filters complicate the parameters selection due to the interrelation among the parameters and various design constraints. Recently, several literatures have been published to discuss the *LCL*-filter parameters design [18]–[23]. In [19], the analytical expressions of harmonic voltages based on Bessel functions was presented, which aims to reduce the grid current harmonics, whereas the optimal capacitance is mainly concerned in [20]. Even if the focuses are dissimilar in diverse design processes, some common principles still exist in different research works irrespective of the various applications. For instance, the selection of *LCL*-filter resonance frequency, the current ripple, the total inductance, the harmonic attenuation rate, and the reactive power absorbed by filter capacitor, etc. It is worth mentioning that, although the inductances of *LCL* filter are reduced compared with the inductances of *L* and *LC* filters, two discrete inductors are still redundant in view of the weight and volume of *LCL* filter. In this scenario, the consideration of magnetic integration techniques in the filter design process is necessary to further minimize the bulky inductors [24]–[26].

Note that, the utilization of the *LCL*-type grid-connected inverters would result in additional stability issues even if *LCL* filters are meticulously designed. Specifically, the stability of the internal current control loop of individual inverter itself is related to the inherent *LCL*-filter resonance peak, so-called the individual internal stability. Also, the overall system stability may be deteriorated due to the underlying external interaction resonances between the inverter and the weak grid as well as among paralleled inverters, namely, the external stability of the inverter [27]–[29].

With respect to the methods for improving the internal stability of individual inverter, the passive damping (PD) methods can be applied by adding resistors in series or parallel with the *LCL*-filter branches [30]. However, the inevitable damping losses and degraded harmonics attenuation ability in high-frequencies are yielded due to the presence of dissipated components. Furthermore, the complex PD methods are alternative to diminish the power losses and regain the filtering performance [31], [32], yet the size and weight of filters are increased, arising from the additional passive components. Besides, by inserting a digital filter in the forward path of current control loop, the filter-based damping method is also applicable to suppress the *LCL*-filter resonance peak [33], without extra sensors, whereas the robustness of this method is poor. In this case, an additional state variable can be fed back for both damping the *LCL*-filter resonance peak and increasing the system robustness, which emulates a physical resistor in the *LCL*-filter branch [34], i.e., an virtual impedance. The analytical expression and connection type of virtual impedance are dependent on the feedback variable and coefficient [35], [36].

As for the external stability, generally, the stability analysis approaches can be roughly categorized into the state-space method in time-domain and the impedance-based method in frequency-domain [37]. In [38], the state-space model of the inverter system is established to investigate the stability, in which case the stability analysis and the design of the system parameters in time-domain are straightforward for the control process. Yet, this method is deficient and inconvenient for AC DPGS due to the requirement of detailed system parameters, and intrinsically reveals the variation of internal state variables for internal stability. Conversely, the impedance-based method is used to evaluate the stability by exploring the terminal characteristics of the system, namely, whether the ratio of the inverter output impedance to the grid impedance satisfies the Nyquist stability criterion (NSC) [39]. The impedance-based stability analysis method has been widely utilized in recent years [40]–[44], and the study in [45] indicates that the instability would arise in the case of weak grid due to the interaction between the inductive grid impedance and the capacitive output impedance of the current-controlled inverter.

Normally, the inverter output impedance can be theoretically derived by employing the equivalent transfer functions [46], [47] or small-signal linearization method [48], and can

also be obtained by means of the impedance measurement through injecting the perturbation signals into the grid voltage and capturing the corresponding responses, in which case the system is regarded as a black box [49], [50]. As for the grid impedance, its information is usually acquired by impedance measurement techniques by superposing small perturbations on the current reference signals. Also, the grid impedance needs to be identified in real time to predict the global stability of the interconnected system, so that diminish the effect of the time-varying characteristics of grid impedance [51], [52].

The above introduction aims to discuss the existing stability problems of *LCL*-type grid-connected inverters and how to solve and assess these issues. Thereafter, this paper presents a comprehensive overview on the state-of-the-art techniques of *LCL*-type grid-connected inverters, including the *LCL*-filter design, the internal and external stability of inverters.

The remainder of this paper is organized as follows. Section II reviews the generalized parameters design constraints and magnetic integration techniques of *LCL* filters. Subsequently, in order to solve the internal instability induced by the *LCL*-filter resonance peak, the damping methods, including the passive damping methods, filter-based damping methods and state-feedback-based damping methods are summarized in Section III, and the influence of control delay on the system stability and the corresponding countermeasures are also discussed. Moreover, Section IV gives an overview on the impedance-based stability analysis, impedance modeling methods, online impedance identification techniques and the interactive stability analysis of the paralleled inverters. Finally, Section V concludes this paper and the future research trends are presented.

II. LCL-FILTER DESIGN

As an interface between the inverter and the grid, the *LCL* filter improves the quality of injected grid current and voltage at the point of common coupling (PCC), thereby avoiding grid oscillation or even destabilization caused by the harmonics pollution issues to some extent [18]. Specifically, the preferred properties of *LCL* filter are summarized as follows [53]:

1) High current ripple rejection [30], [54]–[56].
2) Fast dynamic response [18], [20], [53], [57].
3) Low voltage drop across the filter [18], [20], [53], [57].
4) High power factor [18], [57].
5) Low volume and weight [18], [20], [30], [53], [57].

Fig. 2 shows the equivalent circuit of *LCL*-type grid-connected inverter system, where L_1 and L_2 are the inverter-side and grid-side inductors, respectively, C is the filter capacitor, Z_g is the grid impedance, i_1 and i_2 are the inverter-side and grid-side currents, respectively, i_C is the capacitor current, u_{inv} is the inverter output voltage, u_{pcc} is the voltage at PCC, u_C is the capacitor voltage, and u_g is the grid voltage.

The high-order characteristics of the *LCL* filter, various constraints and relationships of aforementioned performance requirements complicate the design process. In order to achieve simple and reasonable parameters design,

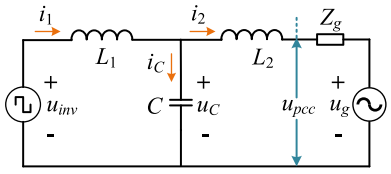

FIGURE 2. The equivalent circuit of the *LCL*-type grid-connected inverter system.

the selection basis and the influences of parameters on the filtering performance should be concerned. Meanwhile, the magnetic integration techniques are worth considering for reducing the device volume or constructing the higher-order output filters.

A. PARAMETERS SELECTION FOR LCL FILTER

The selected parameters mainly include the filter capacitor C, the total inductance L_T, the inverter-side inductance L_1, the harmonic attenuation rate δ and the resonance frequency f_r.

Generally, the capacitor branch is the dominant flow path of high-frequency current harmonics. The selection of capacitor value should achieve a tradeoff between the power factor (PF) and the harmonics attention ability of *LCL* filter [57], thus the reactive power stored in the capacitor is usually less than 5% of the rated active power of the inverter in this case [18], [30]. In addition, the capacitor value of wye connection is three times of that of delta connection in three-phase system [58], [59]. With respect to the total inductance L_T, the fundamental voltage drop across the filter inductors should be less than 10% of grid voltage [18]. Note that, the high dc-link voltage is needed to assure the current controllability in the case of large L_T, which leads to high switching losses [60]. As for the inverter-side inductor, its inductance is mainly related to the inverter topology [55], [61], modulation index [61], modulation strategy [62], and current ripple requirement [55], [63], etc. Commonly, the allowable maximum current ripple should be appropriately selected for obviating the inductor saturation problems [64], and the L_1 is inversely proportional to maximum current ripple [63]. In addition, the resonance frequency f_r should be in the range of $10f_0 \leq f_r \leq f_{sw}/2$ [18], where f_0 is the fundamental frequency of grid voltage, and f_{sw} is the switching frequency.

Specifically, the generalized design constraints are summarized in Table 1 to facilitate the parameters selection of *LCL* filter, where U_{rms} is the RMS of fundamental line-to-line grid voltage, P_n is the rated active power of the inverter, U_{dc} is the dc-link voltage, I_{rated} is the rated current of the inverter, $i_{1\ sw}$ and $i_{2\ sw}$ are the switching frequency current harmonics across L_1 and L_2, respectively, ω_{sw} is the switching angular frequency.

In general, the initial conditions should be determined ahead of the design process, including $U_{rms}, P_n, f_{sw}, f_0, I_{rated}$. Then the parameters selection of *LCL* filter can be implemented by using the following step-by-step design procedure proposed in [18].

TABLE 1. Constraints for choosing *LCL*-filter parameters.

Parameters of the *LCL* filter	Constraints		Impact of parameters on filter performance
Filter capacitor C [18], [57]	$C<5\%\frac{P_n}{2\pi f_0 U_{rms}^2}$		• Large C results in low power factor • Small C requires large inductance
Total inductance L_T [18], [60] (L_T=L_1+L_2)	$L_T \le 10\%\frac{U_{rms}^2}{2\pi f_0 P_n}$		• Large L_T results in large voltage drop, small current ripple and PF, poor dynamic response and high cost
Inverter-side inductance L_1	Single-phase inverter with unipolar SPWM, r = 8 [30], [54]	$L_1 \ge \frac{U_{dc}}{(20\%\sim30\%)I_{rated} r f_{sw}}$	• Large L_1 results in small current ripple, high voltage drop and cost
	Single-phase inverter with bipolar SPWM, r = 2 [30]		
	Three-phase two-level inverter using SPWM or SVM, m_i is the modulation index [61]	$L_1 \ge \frac{\sqrt{3}}{12}\frac{U_{dc}}{30\% I_{rated} f_{sw}} m_i$	
Harmonic attenuation rate δ [18] $\delta=\left\|\frac{i_{2sw}}{i_{1sw}}\right\| = \frac{1}{\left\|1+a_L(1-L_1 C\omega_{sw}^2)\right\|}$, $\omega_{sw} = 2\pi f_{sw}$	δ=20%		• Small δ corresponds to low THD
Resonance frequency f_r [18], [58] $\omega_r = 2\pi f_r = \sqrt{(L_1+L_2)/L_1 L_2 C}$	$10f_0 < f_r < 0.5 f_{sw}$		• Small f_r results in narrow control bandwidth • Large f_r results in resonance peak near f_{sw}

Step 1: Determine the maximum total inductance L_{Tmax}.

Step 2: Select L_1 greater than the minimum inverter-side inductance $L_{1\ min}$.

Step 3: Determine the maximum capacitor value C_{max}. The initial C can be chosen as one half of C_{max} to reduce the iteration design process.

Step 4: Select original harmonic attenuation rate δ as 20% for a tradeoff between the total harmonic distortion (THD) of grid current and filter costs [18]. Then the L_2 can be determined according to the δ and the ratio a_L between L_2 and L_1, i.e., $a_L = L_2/L_1$. Besides, the L_2 can also be directly chosen by setting $a_L = 1$, in which case the size of the passive components can be minimized, whereas $a_L = 1$ corresponds to the minimum harmonics attention [57]. Note that, if the sum of L_2 and L_1 is greater than the L_{Tmax}, a new design procedure should be easily implemented by increasing C [58].

Step 5: Verify that the resonance frequency f_r is within the reasonable range [18]. If f_r is lower than $10f_0$, the capacitor value in Step 3 should be reduced. Conversely, if f_r is higher than $f_{sw}/2$, the capacitor value or f_{sw} should be increased [58].

Step 6: Check that the THD of grid current is lower than 5%. If the THD is higher than 5%, the δ should be properly reduced with a new design procedure [58].

To conclude, the parameters selection of *LCL* filter is a iteration process until all the constraints are satisfied. After completing the above steps, the final parameters of *LCL* filter can be determined, then the magnetic design of inductors needs to be considered in the next design procedure, such as core materials and size, winding turns, air gaps and core shapes.

B. MAGNETIC INTEGRATION TECHNIQUES FOR LCL FILTER

As for the conventional *LCL* filters, the utilization of two discrete magnetic cores causes bulky filter inductors. In order to reduce the weight and size of filters, two discrete inductors can be integrated into one magnetic core, where the magnetic flux of the two inductor windings in the common path is reversed to reduce the total magnetic flux of common core, thus the cross-sectional area of common core is diminished, thereby decreasing the volume of the overall magnetic core [30]. Conversely, the magnetic flux direction of two windings in the common core can also be identical, in which case the coupling effect between L_1 and L_2 can be intentionally maximized to construct the equivalent high-order filters, without extra trap inductors [65]. The magnetic integration techniques are mainly related to the selection of the magnetic materials, core shapes, adopted wires and winding methods.

In comparison, the soft magnetic materials, such as ferrites, laminated silicon steel, powder core, amorphous alloys and nanocrystalline materials, are generally utilized in the filter inductors of power electronic devices [66]. It is noteworthy that high saturation flux density and relative permeability of magnetic materials contributes to diminish the winding turns of inductors [26], and high Curie temperature guarantees the stable inductance [67]. Specifically, the ferrite materials exhibit low core losses and saturation flux densities, which are unsuitable for the large current applications [66]. Moreover, the thin laminated silicon steel is commonly used on account of the low eddy current losses and lighter weight. The powder core is also the superior material owing to its low eddy current losses and stable inductance against the temperature variation. However, the distributed air gap existed in powder core may cause additional fringing effect losses [67], and their nonlinear current-dependent inductance characteristics would affect the effective *LCL*-filter design [68]. Also, the amorphous alloys and nanocrystalline are alternative materials due to the low core losses and high saturation magnetic flux densities, yet the high cost may be unacceptable in the practical applications [66]. Actually, the utilization of copper foils [69] and Litz wires [26], [66] can further reduce the copper losses caused by skin effects.

The different core structures and the corresponding equivalent circuits are shown in Figs. 3-5, including the EIE-, UIU- and EE-type cores, where Φ_1, Φ_2 and Φ_c are the magnetic fluxes generated by inverter-side current i_1, grid-side current i_2, and capacitor current i_C, respectively, the air-gaps (g_1 and g_2) and winding turns (N_1, N_2 and N_c) can be adjusted to obtain desired inductances.

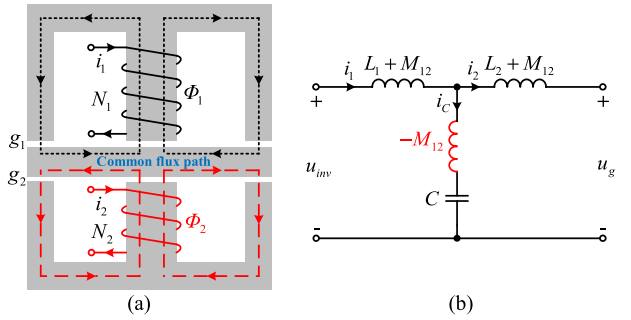

FIGURE 3. Integrated *LCL* filter with positive coupling effect in [69] and [70]. (a) EIE-type core structure. (b) Equivalent circuit.

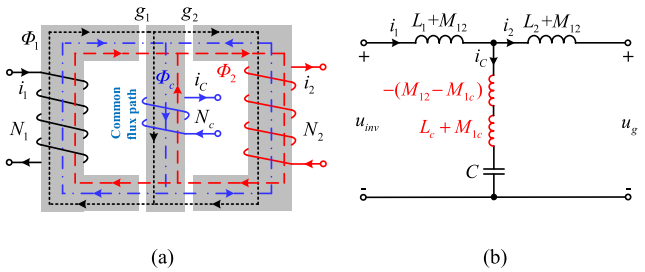

FIGURE 4. Active magnetic decoupling for the positive coupled *LCL* filter in [71]. (a) UIU-type core structure. (b) Equivalent circuit.

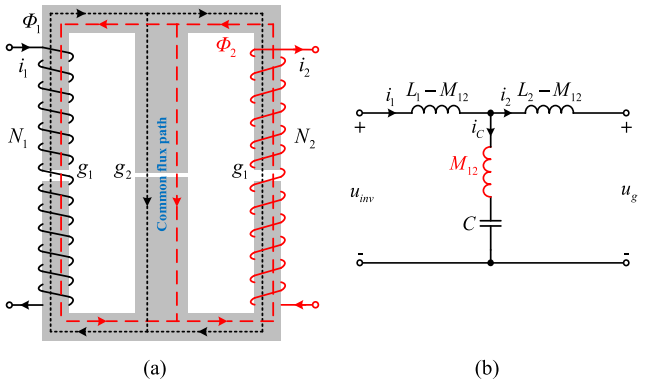

FIGURE 5. Constructed *LLCL* filter with negative coupling effect in [65]. (a) EE-type core structure. (b) Equivalent circuit.

As illustrated in Fig. 3, the integrated EIE-type core structure is proposed in [70] to reduce the volume and weight of filter, where the positive coupling effect between L_1 and L_2 introduces a negative mutual inductance $-M_{12}$ in the capacitor branch. Consequently, the high-frequency attenuation slope of the integrated *LCL* filter is simultaneously degraded due to the $-M_{12}$. In this way, the properly decreased coupling coefficient can be employed to ensure effective filtering performance [69]. In order to counteract the $-M_{12}$, an active magnetic decoupling winding on the I-type core is applied in the UIU-type core structure [71], i.e., $L_c + 2M_{1c} = M_{12}$, as depicted in Fig. 4, where L_c is the self-inductance of the decoupling winding, and $M_{1\,c}$ is the mutual inductance. Moreover, by integrating two inductors into the EE-type core structure with negative coupling effect between inductor windings, a positive mutual inductance M_{12} is introduced in the capacitor branch to construct an equivalent *LLCL* filter in [65], as shown in Fig. 5. Then, the strong switching-frequency harmonics attenuation can be achieved. However, the double volume and weight of common flux path are required to avoid magnetic saturation in this case.

For the sake of reasonable filter design, the specific design aspects about inductors selection are presented in Table 2. To conclude, the positive coupling effect between the inductor windings should be significantly reduced for improving the filtering performance of *LCL* filter, which can be realized by decreasing the coupling coefficient of windings. Conversely, in order to construct an equivalent high-order filter, the negative coupling effect between L_1 and L_2 needs to be effectively maintained for introducing a positive mutual inductance in the capacitor branch. Besides, the soft ferrites and silicon steels are mostly applied due to the advantage of low cost.

Indeed, from the above discussion on the parameters selection and inductors integration of *LCL* filter, the quality of injected grid current can be improved while increasing the power density of the system, with reasonable filter design. In this scenario, the implicit menace caused by PWM to the conventional grid can be eliminated, namely, obviating the grid oscillation or even destabilization induced by the harmonics pollution. Despite all that, the instability of individual inverter itself induced by the inherent *LCL*-filter resonance peak cannot be exempted irrespective of the deliberate filter design, thus the additional countermeasures are naturally required to damp the resonance peak.

III. DAMPING METHODS FOR INTERNAL STABILITY

It is well-known that, the stability of the internal current control loop of individual inverter is aggravated due to the *LCL*-filter resonance peak. Accordingly, the various damping methods can be employed to increase the system damping for solving the resonance problem, including the passive damping (PD) methods, the filter-based damping methods and the state-feedback-based damping methods. The main application disadvantage of PD methods is the inevitable power losses, and the unfavorable factor that affects the latter two damping methods is mainly due to the digital control delay, which would be discussed as follows.

A. PASSIVE DAMPING METHODS

In order to suppress the *LCL*-filter resonance peak, six typical PD methods can be utilized by adding the series or paralleled resistors into the *LCL* filter branches, as shown in Fig. 6. The R_1, R_3 and R_5 are the damping resistors in series with

TABLE 2. Specific aspects about inductors selection of *LCL* filters.

Specific aspects		Advantages	Disadvantages	Applications
Core materials [66], [72]	Ferrites	• Low cost • Low core losses • High resistivity	• Fragile • Low saturation flux density • Low Curie temperature	• Low-current applications
	Laminated silicon steel	• Low eddy current losses • Reduced acoustic noise • High Curie temperature	• Fragile • Reduced saturation flux density • Reduced life time of laminated materials	• Low-current applications
	Powder core	• Low eddy current losses • High saturation flux density • High resistivity and Curie temperature	• Cause fringing effect losses • Electromagnetic interference	• High-current applications
	Amorphous alloys	• Low core losses • High saturation flux density	• Low Curie temperature • High cost	• High-current applications
	Nanocrystalline materials	• Low eddy current losses • High saturation flux density • High Curie temperature	• High cost • Cause fringing effect losses	• High-current applications
Core shapes and Winding methods	EIE-type with positive coupling [69], [70]	• Reduced volume and weight • Reduced core losses	• Degraded high-frequency attenuation ability	• Integrate single-phase or three-phase *LCL* filter
	EE-type with negative coupling [65]	• Strong attenuation ability for switching-frequency harmonics	• Poor attenuation ability away from the switching frequency • Lack of design flexibility	• Construct equivalent *LLCL* filter
	UIU-type with positive coupling [71]	• Ensure harmonics attenuation ability of -60dB/dec	• Increased windings • Stringent design requirement	• Decoupling the integrated *LCL* filter
Adopted wires	Copper foils [69]	• High space utilization • Small leakage inductance	• High cost • Difficult manufacturing process	• High-current applications • Less winding turns
	Litz wires [26], [66]	• Easy winding • Low eddy current losses	• Poor overload capability	• Low-current applications • More winding turns

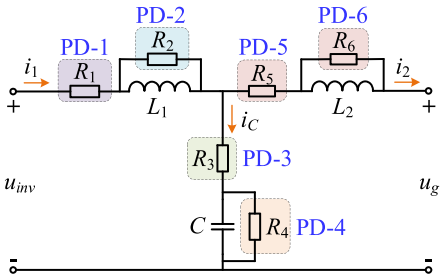

FIGURE 6. The placements of damping resistor of six typical PD methods [30], [73].

L_1, C and L_2, respectively, R_2, R_4 and R_6 are the damping resistors in parallel with L_1, C and L_2, respectively. Moreover, R_1 and R_5 can also be regarded as the equivalent resistances of L_1 and L_2, respectively. The bode diagrams of six typical PD methods are shown in Fig. 7, and the transfer functions corresponding to the various damping methods are also incorporated in Fig. 7.

Corresponding to the PD methods in Figs. 7(b), 7(c) and 7(f), the high-frequency attenuation slope is reduced in comparison with that of undamped *LCL* filter since the additional zeros are contained in the transfer functions [32]. In Fig. 7(a) and Fig. 7(e), the attenuation ability of high-frequency harmonics is unaffected, whereas the large damping losses are caused by PD-1 and PD-5 owing to the directed path of the power flux through R_1 and R_5. Meanwhile, the utilization ratio of DC voltage and the dynamic tracking performance are weakened due to the presence of diminished low-frequency gain, thus PD-1 and PD-5 are not recommended. Besides, the comparatively large resistances are required in PD-2 and PD-6 to achieve PD, with decreased harmonics attenuation ability. Notably, the filtering performance of PD-4 is the best among the six PD methods, with invariable frequency characteristics, yet the damping losses are relatively high due to the effect of PCC voltages [30].

From the perspective of power losses, effective damping and filtering performance, the PD-3 using a small resistance is most appropriate in comprehensive comparison with other typical PD methods, despite of the degraded high-frequency harmonics attenuation ability. In [74], the minimum value of R_3 is chosen as 20% of the capacitor impedance at the resonance frequency to ensure sufficient stability margin of the system, and the maximum value of R_3 is selected as the capacitor impedance at the switching frequency to guarantee effective high-frequency harmonics attenuation.

Concretely, the comparison of the typical PD methods and the selection conditions of the damping resistances are presented in Table 3, where ω_r is the resonance angular frequency of the *LCL*-filter, k_p is the proportional coefficient of current controller, and K_{PWM} is the gain of the inverter bridge.

Obviously, the power losses caused by PD-3 are inevitable no matter in high or low power applications. The currents through the damping resistor R_3 can be sorted into the fundamental, switching harmonics and resonance components, and the power losses are mainly caused by the fundamental and resonance currents [75]. Based on PD-3, several complex PD

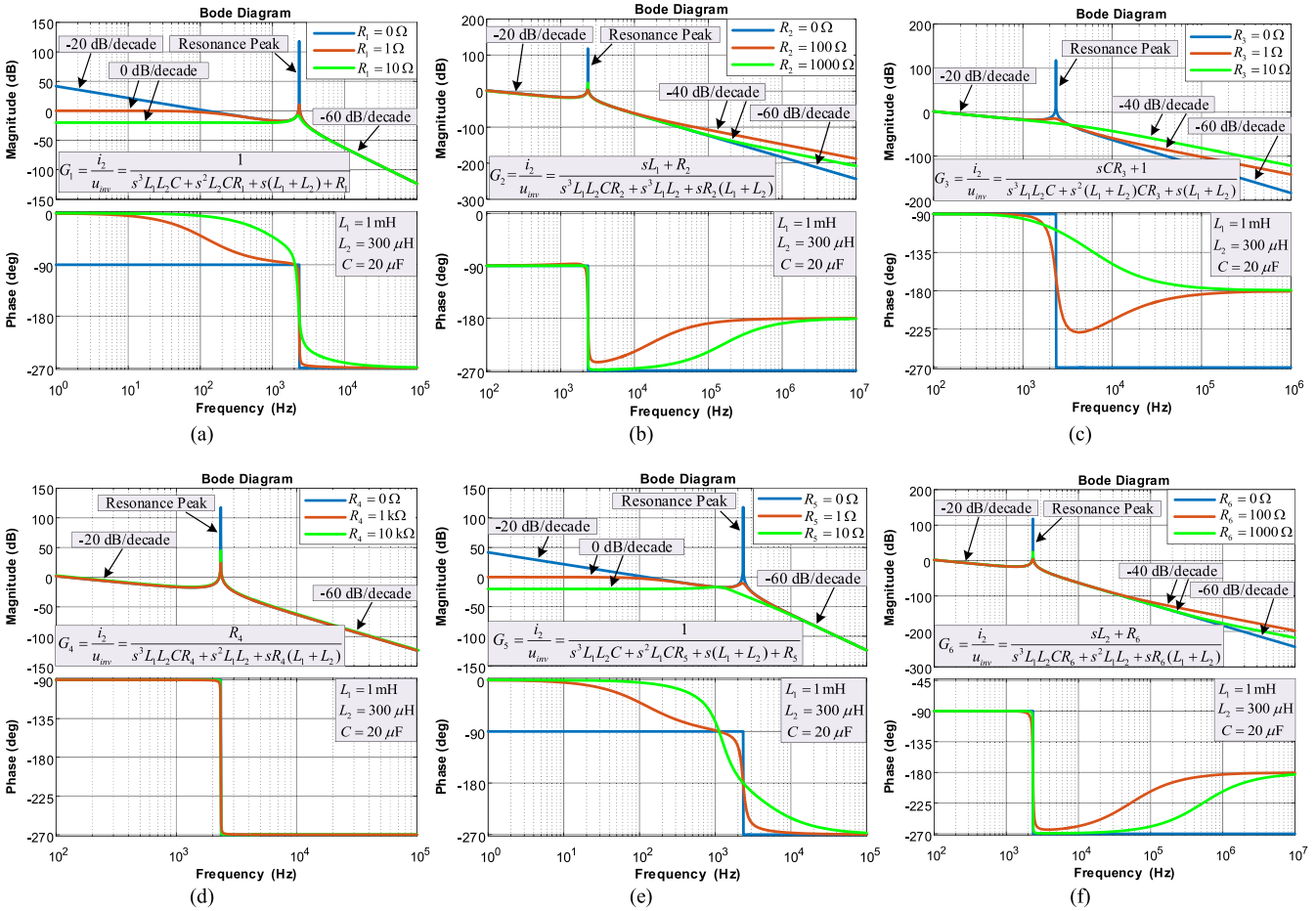

FIGURE 7. The bode diagrams of six typical passive damping methods [30]. (a) PD-1. (b) PD-2. (c) PD-3. (d) PD-4. (e) PD-5. (f) PD-6.

TABLE 3. Comparison of the typical passive damping methods.

Damping methods	Damping resistances selection	Compared with the undamped *LCL* filter	
		Merits	Drawbacks
PD-2 [73]	$0 < R_2 < \frac{(L_1+L_2)+\sqrt{(L_1+L_2)^2+4K_{PWM}^2k_p^2L_1C}}{2K_{PWM}k_pC}$	• Low-frequency gain is unaffected	• Degraded high-frequency harmonics attenuation ability • Cause damping losses
PD-3 [74]	$\frac{1}{6\pi}\frac{L_2}{L_1}\frac{f_{sw}}{f_r}\frac{1}{C\omega_r} \le R_3 \le \frac{1}{2\pi f_{sw}C}$	• Low-frequency gain is unaffected • Only need a small damping resistor	• Degraded high-frequency harmonics attenuation ability • Cause damping losses
PD-4 [73]	$0 < R_4 < \frac{L_1+L_2}{K_{PWM}k_pC}$	• Frequency characteristics are unaffected • Superior damping performance	• Large damping losses • Poor ability of reference tracking and disturbance rejection
PD-6 [73]	$0 < R_6 < \frac{(L_1+L_2)+\sqrt{(L_1+L_2)^2+4K_{PWM}^2k_p^2L_2C}}{2K_{PWM}k_pC}$	• Low-frequency gain is unaffected • Fast dynamic response • Superior disturbance rejection ability	• Degraded high-frequency harmonics attenuation ability • Large damping losses

methods are proposed to reduce a certain amount of damping losses while retaining high-frequency harmonics attenuation ability [56], which are realized by adding the shunt capacitor or inductor in the capacitor branch, as indicated by the passive elements marked in red color shown in Fig. 8.

In Fig. 8(a), the power losses caused by the fundamental current are minimized owing to the low impedance path, i.e., $\omega_0 L_d \ll R_d$ [56]. In addition, the damping resistor R_d should be the dominant path of resonance current to increase the system damping, i.e., $R_d \ll \omega_r L_d$ [74]. Based on the Fig. 8(a), the additional C_d in Fig. 8(b) is employed to decrease the power losses caused by switching-frequency current harmonics, and the conditions of $R_d \gg 1/(C_d\omega_{sw})$ and $R_d \ll 1/(C_d\omega_r)$ should be satisfied for low damping

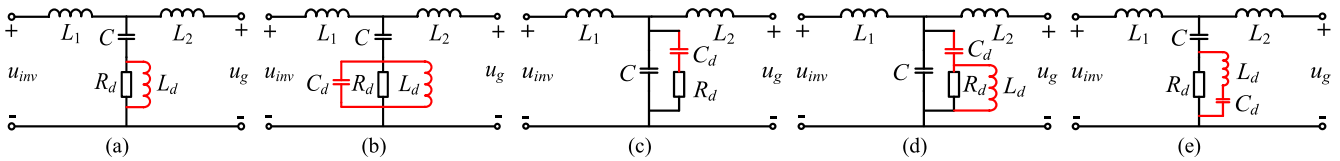

FIGURE 8. The complex PD methods [56], [74]. (a) $C+(R_d//L_d)$. (b) $C+(C_d//R_d//L_d)$. (c) $C//(C_d+R_d)$. (d) $C//(C_d+R_d//L_d)$. (e) $C+(C_d+L_d)//R_d$.

TABLE 4. Performance comparison and parameters selection of the different complex passive damping methods.

Performance compared with PD-3 and parameters selection		$C+(R_d//L_d)$ [74]	$C+(C_d//R_d//L_d)$ [31], [55], [74]	$C//(C_d+R_d)$ [77], [86]	$C//(C_d+R_d//L_d)$ [75]	$C+(C_d+L_d)//R_d$ [78]
Parameters selection		$\frac{R_d}{L_d\omega_0}=\frac{L_d\omega_r}{R_d}$	$\frac{1/(C_d\omega_r)}{R_d}=\frac{R_d}{1/(C_d\omega_{sw})}$	$r_C\sqrt{\frac{1}{r_C}+1}\sqrt{\frac{L_p}{C}}\le R_d\le(1+r_C)\sqrt{\frac{L_p}{C}}$, $L_p=L_1L_2/(L_1+L_2)$, $r_C=\frac{C}{C_d}=1$ [86] $R_d=\sqrt{(L_1+L_2)/(C+C_d)}$, $C=C_d$ [77]	$R_d=\sqrt{(L_1+L_2)/(C+C_d)}$, $L_d=2R_d\sqrt{(L_1//L_2)C}$, $C=C_d$	$R_d=\frac{1}{2\pi f_r C}$, $f_{sw}=\frac{1}{2\pi\sqrt{L_dC_d}}$
Slope of high-frequency attenuation		-40 dB/dec	-60 dB/dec	-60 dB/dec	-60 dB/dec	-40 dB/dec
Power losses caused by various components	Fundamental current	↓	↓	—	↓	—
	Resonance current	—	—	—	—	—
	Switching harmonics	—	↓	↓	↓	↓
Harmonics attenuation of various components	Resonance current	—	—	—	—	—
	Switching harmonics	—	↑	↑	↑	↑

Note: The symbols ↑, ↓ and — represent the increase, decrease and unchanging, respectively.

losses and suitable damping, respectively [74]. Besides, the high-frequency harmonics attenuation slope of the filter shown in Fig. 8(c) is still −60 dB/dec, yet two possible resonance peaks may be induced with the variation of R_d [76]. Moreover, the total capacitance in Fig. 8(c) should be consistent with the capacitance of undamped *LCL* filter, and a tradeoff between the damping performance and the power losses can be attained when the condition $C/C_d = 1$ is satisfied [77]. In Fig. 8(d), the fundamental and switching frequency components of currents are bypassed by the L_d and C_d, respectively, thereby the damping losses on R_d are minimum attributed to the only minor resonance current through R_d [75]. Furthermore, by tuning the $L_d - C_d$ branch at the switching frequency in Fig. 8(e), the switching current harmonic is mostly bypassed due to the introduced low impedance path, thus the power losses are significantly diminished [78].

From the above literatures, a comprehensive comparison between the complex PD methods and the PD-3 is presented to show the better performance of complex PD methods, and the parameter selection conditions of passive components are also summarized, as shown in Table 4.

In summary, the fundamental and the switching-frequency currents through the damping resistor can be bypassed to reduce the power losses. Nevertheless, the resonance current should be flowed through the resistor branch to provide sufficient PD, thus this part of the power losses cannot be diminished. In comparison, the power losses of the complex PD methods in Figs 8(b) and 8(d) are lowest due to the maximum bypass of current components. Moreover, the approach with only an additional capacitor in Fig. 8(c) is easiest to be implemented among these complex PD methods, since the consideration of the complicated inductor design is not required in this case.

However, the overall complexity of the circuit topologies and parameters design, and the cost and volume of *LCL*-filter are increased with the adoption of complex PD methods, and the damping losses cannot be eliminated completely. In this case, the methods for increasing the system damping by modifying the control algorithms have become increasingly popular in recent years, without any passive components and power losses.

B. FILTER-BASED DAMPING METHODS

By inserting a digital filter with special function in the forward path of current control loop, the *LCL*-filter resonance peak can be damped by using the filter-based damping method, without any additional sensors and passive components. The filters mainly include the notch filter [33], [79]–[84], the low-pass filter (LPF) [33], and the all-pass filter [85].

The control block diagram of the filter-based damping methods is shown in Fig. 9, and the close-loop control scheme

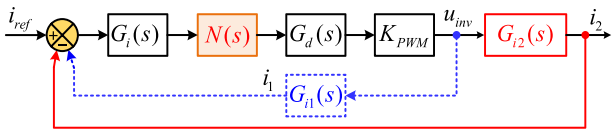

FIGURE 9. Control block diagrams of the filter-based damping methods with different current feedback strategies (blue dotted line represents the ICF, and red solid line represents the GCF) [33].

for reducing the steady-state error can be either inverter-side current feedback (ICF) or grid-side current feedback (GCF).

In Fig. 9, the digital filter represented by $N(s)$ is usually cascaded to the current controller $G_i(s)$ in the forward path. The $G_i(s)$ is generally a proportional integral (PI) or a proportional resonant (PR) controller, which is employed in dq- or stationary-frame to track the current reference i_{ref} without steady-state error, respectively [87], [88], $G_d(s)$ is the digital control delay, and K_{PWM} is the gain of inverter bridge. The $G_{i1}(s)$ and $G_{i2}(s)$ are the transfer functions from inverter output voltage u_{inv} to inverter-side current i_1 and grid-side current i_2, respectively, which are given as

$$G_{i1} = \frac{i_1}{u_{inv}} = \frac{1}{sL_1}\frac{s^2+\omega_a^2}{s^2+\omega_r^2} \tag{1}$$

$$G_{i2} = \frac{i_2}{u_{inv}} = \frac{1}{sL_1}\frac{\omega_a^2}{s^2+\omega_r^2} \tag{2}$$

where ω_a antiresonance angular frequency introduced by ICF, and ω_r is the resonance angular frequency of *LCL* filter, expressed as

$$\omega_a = 2\pi f_a = \sqrt{\frac{1}{L_2 C}} \tag{3}$$

$$\omega_r = 2\pi f_r = \sqrt{\frac{L_1+L_2}{L_1 L_2 C}} \tag{4}$$

1) NOTCH FILTER

Specifically, the typical transfer function of the notch filter is denoted as follows [79], [82]:

$$N(s) = \frac{s^2+\omega_n^2}{s^2+qs+\omega_n^2} \tag{5}$$

where q is the quality factor of notch filter, and ω_n is the notch angular frequency, $\omega_n = 2\pi f_n$.

The Bode diagrams of ICF and GCF are shown in Fig. 10, with and without the notch-filter-based damping method, respectively. In Fig. 10(a), without considering the control delay, the system using ICF is inherent stable, whereas the system using GCF scheme in Fig. 10(b) is unstable due to the only downward -180° crossing with the gain above 0 dB. After employing the notch filter-based damping method, the positive *LCL*-filter resonance peak is counteracted by the notched resonance peak, with the condition $f_n = f_r$ [33], [80]. Actually, this method is an intrinsical zero-pole cancellation of the system transfer function, i.e., the zero of notch filter and the unstable pole of the *LCL* filter, which attenuates the resonance peak of the magnitude-frequency curve of the system [33].

Note that, a small q corresponds to a narrow rejection bandwidth, which results in high sensitivity to the shifting of resonance frequency [80]. Therefore, considering the variation of the system parameters, the notch frequency is tuned away from the nominal resonance frequency to deal with the shifted parameters in [79] and [82]. In addition, a self-commissioning notch filter is employed in [80] to improve the system robustness, which estimates the resonance frequency and tunes the notch frequency in real time. However, the accuracy of estimation results is still affected by the high dependency on system model. Besides, the phase deviation introduced by the notch filter would result in stability reduction or even instability, thus the denominator phase of notch filter is decreased in [83] to improve the phase margin of the system. Furthermore, the notch effect is also susceptible to

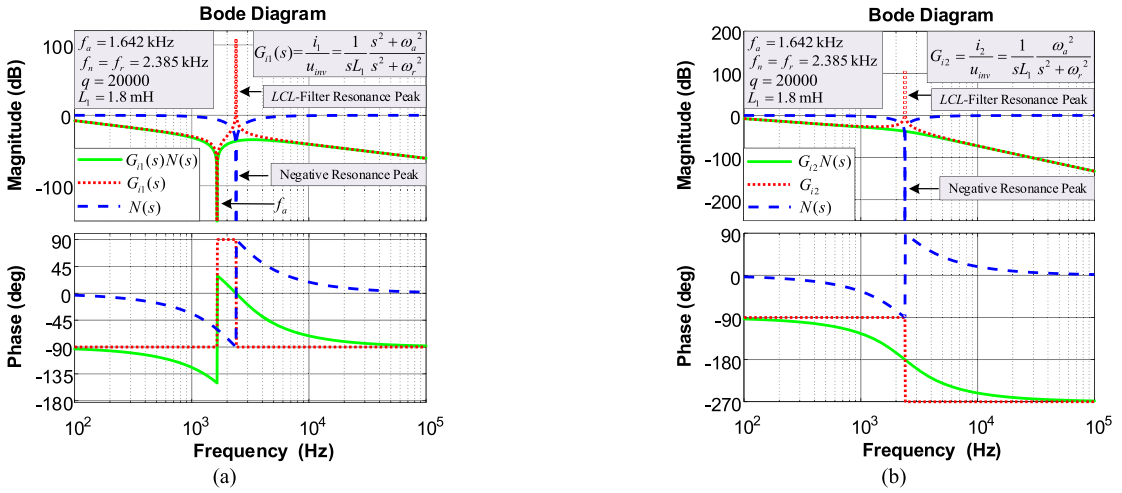

FIGURE 10. Bode diagrams of notch-filter-based damping method with different current feedback strategies [79]. (a) ICF. (b) GCF.

TABLE 5. MeritS and drawbacks of different filter-based damping methods.

Adopted filters	Merits	Drawbacks	Major technologies
Notch filter [33], [79]-[84]	• Simple implementation • Superior damping performance	• Sensitive to the variation of f_r • Small phase margin at low frequencies	• Select the f_n as f_r • Know the resistances of inductors for tuning process
Low-pass filter [33]	• Stabilize system with i_2 feedback at low resonance frequency • Hardly dependent on the grid parameters	• Cutoff frequency limits the control bandwidth • If f_r is close to the closed-loop bandwidth, resonance damping is deficient	• Select the cutoff frequency as f_r • Proper phase lag
All-pass filter [85]	• High-frequency noise is not amplified • Simplify current controller design	• Degraded transient performance (first-order all-pass filter) • Reduced system robustness (second-order all-pass filter)	• Maintain zero open-loop phase at f_r

the parasitic resistances of *LCL* filter, thus the resistances of inductors are necessary to be known for the parameters tuning procedure of notch filter [84].

2) LOW-PASS FILTER

As for the LPF, the selection of the cutoff frequency is a tradeoff between the control bandwidth and the stability margin of the system [33]. Generally, the cutoff frequency can be chosen as the *LCL*-filter resonance frequency. It is noteworthy that, the phase lag caused by LPF contributes to provide proper damping for the system with GCF, and the essence is to shift the phase-frequency curve of the system outside of the unstable frequency region, thereby stabilizing the whole system [33]. The transfer function of the second-order LPF is expressed as

$$N(s) = \frac{\omega_r^2}{s^2 + 2D\omega_r s + \omega_r^2} \tag{6}$$

where ω_r is the resonance angular frequency of *LCL* filter, and D is the damping coefficient, usually selected as $1/\sqrt{2}$.

3) ALL-PASS FILTER

Similarly, the proper phase lag introduced by all-pass filter can also be utilized to enlarge the phase margin of the system at f_r [85]. However, the dynamic performance and robustness of the system are degraded in this scenario. The all-pass filter can be described by equation (7).

$$N(s) = e^{j\phi_d} \tag{7}$$

where ϕ_d is the phase lag introduced by all-pass filter.

From the above literatures, various research works with different filter-based damping methods are systematically reviewed, thus a comprehensive comparison is conducted to show the merits and drawbacks of these methods, as shown in Table 5.

To conclude, the aforementioned filter-based damping methods can be categorized into the approaches based on zero-pole cancellation and phase lag in view of the implementation principles. According to the NSC, the former one is to avoid the gain above 0 dB at the frequency of -180° crossing, and the latter one is to obviate the -180° crossing in the frequency range with a gain greater than 0 dB [33]. It is worth noting that, the damping methods based on the phase lag filters are normally suitable for the GCF, whereas the dynamic performance of the system is degraded in this case due to the reduced control bandwidth. Conversely, the damping of the system with ICF can be increased by using the phase lead filters, in which case the problem of phase overcompensation needs to be precluded. In comparison, the notch filter is more effective due to the strong suppression performance with respect to the resonance peak. The methods based on the phase lead or phase lag are relatively complicated to be implemented, due to the stringent design requirement about that the degree of phase lead or lag should be carefully investigated.

Although the filter-based damping methods show benefits of low cost and simple implementation, the robustness is subjected to the variation of *LCL*-filter resonance frequency. Therefore, an additional state feedback is generally adopted to improve the system robustness.

C. STATE-FEEDBACK-BASED DAMPING METHODS

In addition to the original closed-loop control variables used to reduce the steady-state error of the system, an extra state variable can also be fed back to increase the system damping. The supplemental feedback variable for increasing the system damping can be the capacitor current feedback (CCF), the capacitor voltage feedback (CVF), the ICF or the GCF. The control block diagram of the system with different states feedback is illustrated in Fig. 11.

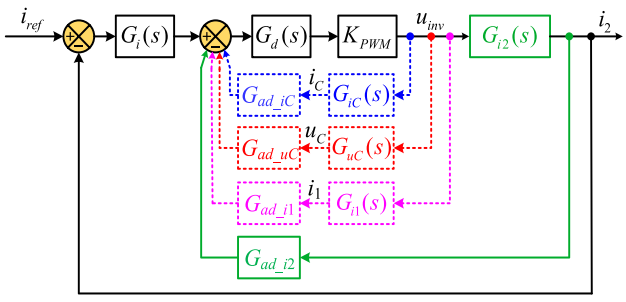

FIGURE 11. Control block diagram of various state-feedback-based damping methods [89].

In Fig. 11, the G_{ad_iC}, G_{ad_uC}, G_{ad_i1} and G_{ad_i2} are the feedback coefficients to increase damping actively. The $G_{iC}(s)$ and $G_{uC}(s)$ are the transfer functions from inverter output voltage u_{inv} to i_C and u_C, respectively, which are expressed as

$$G_{iC} = \frac{i_C}{u_{inv}} = \frac{1}{sL_1}\frac{s^2}{s^2+\omega_r^2} \tag{8}$$

$$G_{uC} = \frac{u_C}{u_{inv}} = \frac{1}{L_1C}\frac{1}{s^2+\omega_r^2} \tag{9}$$

Note that, the state-feedback-based damping method is equivalent to a virtual impedance in series or parallel with the *LCL*-filter branch, so-called virtual impedance-based method. Thereafter, the different states feedback and their corresponding virtual impedances are discussed as follows.

1) CAPACITOR CURRENT FEEDBACK

In Fig. 11, the system can be stable with increased resonance damping when the G_{ad_iC} is a proportional coefficient [90]. In this scenario, the CCF is equivalent to a virtual impedance in parallel with the filter capacitor. The virtual impedance in the case of proportional feedback can be modeled as follows [91], [92]:

$$Z_{VI}(s) = R_{VI}//(jX_{VI}) = \frac{L_1}{K_{PWM}CG_{ad\_iC}G_d(s)} \tag{10}$$

Specifically, the resonance frequency would be shifted due to the virtual reactance X_{VI} [91], [92], and the *LCL*-filter resonance peak is damped attributed to the virtual resistor R_{VI}. Yet, the damping method is invalid when the R_{VI} is negative, which can be solved by adopting the PI feedback [93] or the first-order HPF feedback [94] of i_C. Moreover, the resonance damping can also be achieved when the G_{ad_iC} is a second-order HPF with R_{VI} gain [28], in which case the CCF can be equivalent to a virtual pure resistor R_{VI} in series with the filter capacitor. However, the high-frequency noise would be easily amplified by the approximate derivative characteristics of HPF, and the control algorithm is more complicated than that of proportional feedback.

2) CAPACITOR VOLTAGE FEEDBACK

In addition, the resonance damping can also be yielded by applying the first-order derivative feedback of capacitor voltage since $i_C(s) = sCu_C(s)$ [90], which emulates a physical impedance in parallel with the filter capacitor [95]. However, the direct derivative operation is difficult to be implemented in digital controllers. Hence, the indirect derivation, such as the HPF [96], [97] and the lead-lag network [98] can be adopted to approximate the direct derivation. Nonetheless, a large phase error introduced by the HPF leads to insufficient derivation at high frequency, and the lead-lag network is only suitable for strong grid. Another better indirect derivation schemes are the nonideal generalized integrator (GI) [99] and the quadrature-second-order generalized integrator (Q-SOGI) [100], which avoid the problem of noise amplification at high frequency. Nevertheless, the practical application is limited due to the complex algebraic process of GI and low robustness of Q-SOGI. In this way, a first-order backward-lead differentiator and a second-order Tustin-notch-filter are proposed in [89] to match the ideal derivative nature, with the advantages of direct discretization and simple implementation. Additionally, the proportional feedback of capacitor voltage can also be used to provide proper resonance damping, which simulates a virtual resistor in parallel with the filter capacitor [101], yet the damping effect of this method is deficient compared with that of derivative feedback.

3) INVERTER-SIDE CURRENT FEEDBACK

Generally, the ICF is utilized as the overcurrent protection for the inverter [12]. As for increasing the system damping, the proportional ICF is feasible to simulate an equivalent virtual impedance in series with L_1 [102]. Nonetheless, the additional resonance might be excited between C and L_2 due to the grid voltage harmonics, and the dynamic tracking performance of this strategy is also degraded because of the decreased low-frequency gain [103]. Furthermore, the inverter-side current and grid-side current can be collaboratively controlled by means of weighted average control (WAC), which simplifies the system order from third-order to first-order in this case [104], [105]. The control block diagram of the WAC is illustrated in Fig. 12, where β and $(1-\beta)$ are the weight values of i_1 and i_2, respectively, and i_{WA} is the weighted average current. The coefficient β is defined by (11) [104], [106].

$$\beta = \frac{L_1}{L_1+L_2+L_g} \tag{11}$$

where L_g is the grid inductance. Apparently, the robustness of WAC is susceptible to the variation of grid inductance.

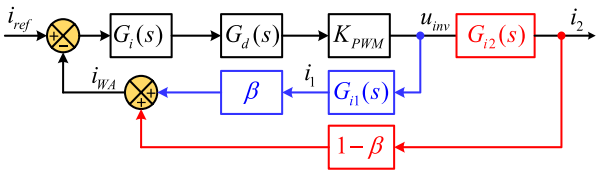

FIGURE 12. Control block diagram of the weighted average control [104], [106].

Without considering the effect of control delay, the WAC of the currents can be regarded as a virtual impedance in parallel with the filter capacitor, in which case the high-pass characteristics of the virtual impedance enable a low impedance flow path for high-frequency harmonics equivalently [103], and the virtual impedance is modeled as follows:

$$Z_{VI}(s) = \frac{L_1}{C(1-\beta)G_i(s)} \tag{12}$$

In addition, the ICF scheme can also be regarded as a virtual impedance in series with L_1 when G_{ad_i1} is a first-order HPF, [107]. Hence, the expression of virtual impedance is given as

$$Z_{VI}(s) = R_{VI} + jX_{VI} = K_{PWM}G_{ad\_i1}(s) \tag{13}$$

TABLE 6. Comparison of state-feedback-based damping methods.

Feedback signals	Feedback coefficients	Merits	Drawbacks	Major technologies
i_C (capacitor current)	Proportional feedback [13], [91], [92]	• Simple implementation • Superior damping performance	• Impair the phase margin of system • Degraded transient response	• Select G_{ad_iC} with a tradeoff between the gain margin and phase margin
	Proportional integral feedback [93]	• Simple implementation • Improved robustness	• Integral term would accumulate the noise	• Replaced by proportional feedback of i_C plus proportional feedback of u_C
	First-order HPF [94]	• High robustness • Mitigate phase lag	• Amplify high-frequency noise • Cause phase error • Reduce system bandwidth	• Select the proper cutoff frequency of HPF firstly
	Second-order HPF [28]	• Stabilize current loop • Strengthen interaction stability between the inverter and the grid	• Increase steady-state error • Decrease control bandwidth • Amplify high-frequency noise	• Improve the system robustness against grid impedance variation
u_C (capacitor voltage)	HPF [96], [97]	• Magnitude-frequency characteristic is very similar to ideal derivative	• Enlarged phase error at high frequency • Amplify high-frequency noise	• Discretized by Tustin method
	Lead-lag network [98]	• Small phase error below the frequency of maximum phase shift	• Sensitive to the variation of f_r • Narrow available frequency range	• Discretized by prewarped Tustin method at f_r • Maintain phase lead 90° at f_r
	Nonideal GI [99], [100]	• Wide derivative range • Avoid noise amplification	• Introduce phase error at high frequency • Complex control algorithm	• Discretized by first-order hold method at Nyquist frequency
	Q-SOGI [100]	• Produce accurate phase at f_r • Avoid noise amplification	• Sensitive to the variation of f_r • Narrow available frequency range	• Discretized by prewarped Tustin method at f_r
	Proportional feedback [101]	• Simple implementation	• Deficient damping effect • Low robustness	• Select proportional coefficient deliberately
i_1 (inverter-side current)	Proportional feedback [102], [103]	• Simple implementation	• May excite additional resonance between C and L_2 • Degraded dynamic tracking performance	• Select proper G_{ad_i1} according to the requirements of damping ratio and f_r
	WAC [104]-[106]	• Simplify controller design • Improve the closed-loop control bandwidth	• May appear two resonance frequencies • Sensitive to grid impedance variation	• Improve the system robustness against grid impedance variation
i_2 (grid-side current)	First-order HPF [108]-[111]	• Simple control algorithm • Low hardware cost	• Amplify high-frequency noise • Reduced system bandwidth	• Select the gain and cutoff frequency of HPF eclectically

4) GRID-SIDE CURRENT FEEDBACK

With respect to the GCF, the main merit of this strategy is that only one current sensor is required for both injected grid current tracking and the resonance damping. In [108], it has indicated that the *LCL*-filter resonance peak can be suppressed by applying the second-order derivative feedback of i_2. In order to avoid the implementation difficulty of direct derivation, a first-order HPF with a negative gain is adopted in the additional GCF damping loop in [108]–[111]. However, the control bandwidth of the system is narrowed to some extent [110], and the dynamic performance is poor for the system with low resonance frequency [112]. Note that, the first-order HPF-based damping method is equivalent to a virtual impedance in parallel with the filter capacitor, as follows [107], [113]:

$$Z_{VI}(s) = R_{VI}//(jX_{VI}) = \frac{L_1L_2s^2}{G_{ad\_i2}(s)K_{PWM}} \tag{14}$$

Besides, the feedback coefficient G_{ad_i2} can also be a SOGI with a negative gain, in which case the GCF resembles a virtual impedance Z_{VI} in series with the L_2 [114], and the expression of Z_{VI} can be derived as

$$Z_{VI}(s) = \frac{G_{ad\_i2}(s)G_d(s)K_{PWM}}{s^2L_1C} \tag{15}$$

where the SOGI with the phase lead characteristics is utilized to realize the approximate derivative operation.

In order to analyze the merits and drawbacks of the different state-feedback-based damping methods, a comprehensive comparison is conducted in Table 6. From the above discussion, the placements of virtual impedances in the *LCL*-filter branches can be sorted into four types, as shown in Fig. 13. Referring to the damping effect and the resistor placements of PD methods, it can be concluded that the state-feedback-based damping methods based on Z_{VI3} are the most effective owing to the consistent topology structure with that of PD-4.

Among these damping methods based on Z_{VI3}, the derivative feedback of the capacitor voltage has the advantage of lowest hardware cost since the voltage can be measured for both synchronization operation with the grid and resonance

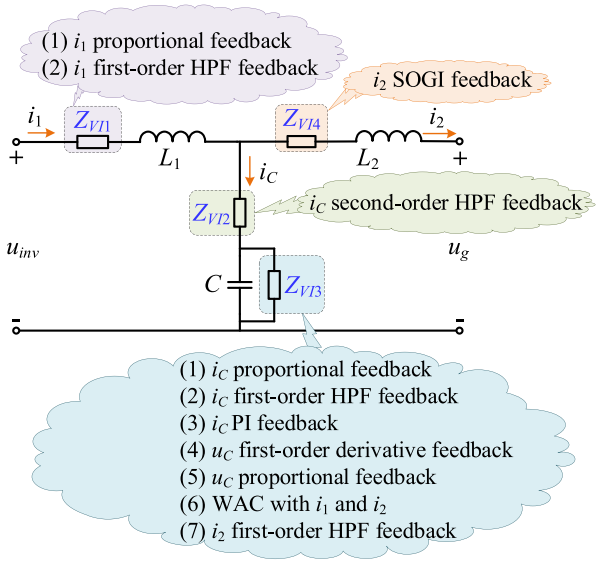

FIGURE 13. Equivalent circuit of state-feedback-based damping methods.

damping, without extra sensor. However, its effectiveness would be easily affected by the high-frequency noise and voltage distortion at PCC, and the damping performance is slightly degraded since the approximate derivation is usually used instead of the direct derivative feedback. Although the number of sensors is minimum for the first-order HPF feedback of current i_2, the effectiveness of this method might be compromised by the effect of amplified high-frequency noise. Besides, in the case of requiring the same number of sensors, the CCF with stronger robustness is preferred to the WAC scheme. In comparison, the proportional CCF is widely applied among the various feedback coefficients due to the merits of simple implementation and sufficient damping performance.

Actually, the single-loop ICF and GCF mentioned in Part B can also be regarded as the virtual impedances in series with L_1 and parallel with C, respectively [116]. It is worth noting that, the *LCL*-filter resonance peak can be damped only under the positive virtual resistor conditions [91], no matter the filter- or state-feedback-based damping methods. Nevertheless, the digital control delay caused by algorithm execution has a significant influence on the characteristics of virtual resistor.

D. APPLICATION ISSUES OF FILTER- AND STATE FEEDBACK-BASED DAMPING METHODS

The total digital control delay T_d composed of computation and PWM delay inherently exists in the current control loop, and the typical values of the total control delay in practical situations are $1.5T_{sm}$ and T_{sm} [117], where T_{sm} is the sampling period. It is well-known that, the phase margin and control bandwidth of the system are decreased due to the phase lag introduced by control delay [118], and the lagging phase can be expressed as follows [119], [120]:

$$\varphi_{delay} = -\frac{f_r}{f_{sm}} \times \left(\frac{T_d}{T_{sm}} + 0.5\right) \times 360^\circ \tag{16}$$

where f_{sm} is the sampling frequency, and f_r is the *LCL*-filter resonance frequency.

Concretely, as for the single-loop ICF, an inherent damping term is embedded in the control loop to stabilize the system in the case of ignoring the control delay [121], whereas the system stability is deteriorated with the consideration of control delay [119]. Hence, the influence of control delay should be reduced for ICF. Conversely, with respect to the single-loop GCF, the system is unstable without control delay, yet inherently stable owing to the proper control delay, also called the inherent damping [122], [123]. This is why the stability of the system with GCF can be improved by means of phase-lag filters [119]. Note that, the system is also unstable if the lagging phase is too large [119]. Essentially, the inherent damping of ICF and GCF is produced by the positive virtual resistor contained in the virtual impedance, whereas the system may be unstable when the virtual resistor is negative [116].

Considering $T_d = 1.5T_{\rm sm}$, the stability regions of single-loop ICF and GCF without any damping measures are shown in Fig. 14, where $f_{sm}/6$ is the critical frequency f_c in this case [124], but the f_c is $f_{sm}/4$ when $T_d = T_{\rm sm}$ [125]. According to the NSC, the system is unstable due to the unequal times of upward and downward -180° crossings in the frequency range with the gain above 0 dB. Corresponding to the unstable regions in Fig. 14, the virtual impedance involves a negative resistor element [116]. Obviously, in order to widening the stable regions for a positive virtual resistor of wider range, the *LCL*-filter resonance frequency can be properly shifted, whereas this method is not practically feasible due to the demand of redesigned *LCL*-filter parameters. Other methods are to adjust the sampling frequency or to control the delay correctly. In Fig. 14, the stable region of ICF can be widen by enlarging the f_c through decreasing the delay effect, but the time delay of GCF should be appropriately increased to lower the f_c for broadening the stable region [115].

For the widely adopted proportional CCF, its stable region is consistent with that of ICF in Fig. 14(a) [125]. Similarly, the negative virtual resistor contained in the virtual impedance is disadvantageous to the system stability [91], [109], [126]. In order to solve the problem of negative virtual resistor, the predictive control techniques, filter-based compensation methods and the modified sampling methods are alternative to diminish the impact of control delay.

The predictive control techniques is to estimate the future value based on the existing information of the system, including the Smith prediction [127], [128], the state observer [129], [130], the linear prediction [127], [131]–[133], etc. In [129], only the inverter-side current is measured for both resonance damping and delay compensation based on the state observer. Theoretically, the value of next step is predicted ahead of time, thus the delay can be fully compensated both by Smith prediction and state observer. Nevertheless, these methods are highly dependent on the accuracy of the system model and the operation conditions, which further increase the calculation burden [127]. Conversely, any information about the system

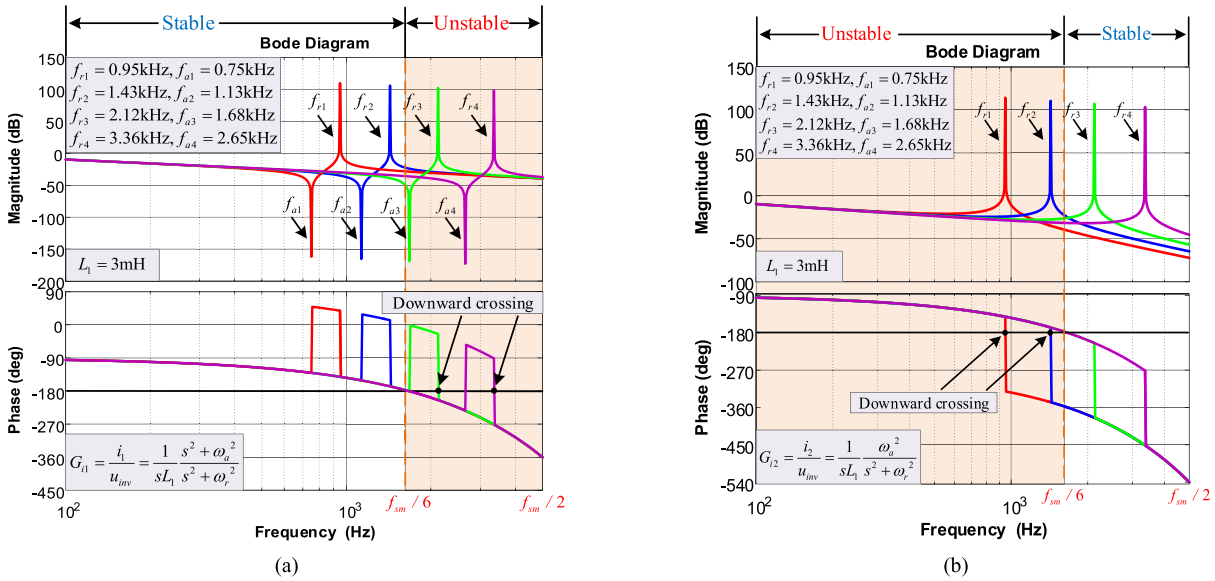

FIGURE 14. Open-loop bode diagrams of different current feedback strategies, with the typical value of $T_d = 1.5\,T_{sm}$ [115]. (a) ICF. (b) GCF.

model is not required when the linear prediction is employed [131], which utilizes the linear extrapolation to estimate the values of the control variables based on the past values. However, the control delay cannot be effectively compensated at high frequency. In comparison, the model-based predictive control methods, i.e., Smith prediction and state observer, are unsuitable for high-order or fast control systems due to the complexity and time consumption, and the linear prediction has the advantages of strong robustness and simple implementation [127].

Furthermore, the filter-based methods are also candidates for delay compensation with the phase lead characteristics, such as the SOGI [115], the lead-lag compensator [134]–[138], HPF [139], [140], and the infinite impulse response (IIR) filter [126], [141]–[144]. In [135] and [136], the lead-lag compensator is inserted into the capacitor current damping loop to compensate the control delay, whereas the compensation effect is largely dependent on the experience of designers [134]. Moreover, an improved delay compensation method based on the impulse area equivalence principle is proposed in [141] to widen the frequency range of phase compensation, which is an intrinsic IIR filter cascading after the delay link. Furthermore, the HPF can also be added into the damping loop to ensure the positive virtual resistor [94], [139], [140]. However, this method may cause over compensation at low-frequency and noise amplification at high-frequency. In conclusion, the noise amplification is the main drawback of the filter-based compensation methods due to the derivative term, and the leading phase should be meticulously determined for a tradeoff between the compensation effect and the over compensation. Among the aforementioned filter-based damping methods, the compensation ability of IIR filter is the best [141], and the HPF is the easiest to be implemented owing to the relatively simple parameters design process.

Unlike the predictive techniques and the filter-based compensation approaches, the modified sampling methods can be more intuitively and easily utilized to reduce delay to a certain extent, which mainly consist of the multiple sampling [95], [107], [145]–[147], shifting the sampling instant [91], [148], shifting the updating instant of reference voltage [149] and dual sampling modes [120]. The control delay can be reduced by multiple sampling method with enlarged sampling frequency [145], thereby the stability region of the system is widen [146]. Yet, this method may result in computation burden on the microprocessor and multiple intersection between the modulation wave and the carrier. It is worth noting that, the PWM delay ($0.5T_{sm}$) cannot be decreased when the sampling frequency is fixed. In this case, the computation delay can be reduced by shifting the sampling instant toward the update instant of the modulation signal, thus the total digital control delay is diminished [91]. However, the sampled signals are susceptible to the aliasing and switching noises. Conversely, the update instant of reference voltage is shifted in [149] to reduce the computation delay, and the PWM delay is compensated by the IIR filter simultaneously. Nevertheless, the noise amplification might be caused due to the infinite gain of IIR filter at Nyquist frequency. Furthermore, according to the size of the duty cycle, a real-time computation method with dual sampling modes is proposed to eliminate the computation delay completely and enhance the noise immunity [120]. However, this method is only suitable for the unipolar SPWM [30], and the algorithm execution process is relatively complicated.

From the aforementioned literatures, the methods for reducing the influence of control delay are systematically reviewed. A comprehensive comparison is conducted to show the merits and drawbacks of various methods, as shown in Table 7. Undoubtedly, the modified sampling methods are most straightforward, next is filter-based compensation

TABLE 7. Merits and drawbacks of the methods for reducing delay influence.

Specific methods		Merits	Drawbacks
Predictive control schemes	Smith prediction [127], [128]	• Compensate delay completely • High control bandwidth	• Sensitive to system parameters • Complicated algorithm
	State observer [129], [130]	• Compensate delay completely • High control bandwidth	• Sensitive to system parameters • Computation burden
	Linear prediction [127], [131]-[133]	• Easy implementation • Robust against parameters variation	• Deficient delay compensation at high frequency • Limited control bandwidth
Filter-based compensation methods	Lead-lag compensator [134]-[138]	• Simple implementation • Approximate a differentiator at f_r	• Relatively complex parameters design • Sensitive to the variation of f_r • Exist phase error below 90°
	SOGI [115]	• Simple implementation • High robustness	• Noise amplification at high frequency • Relatively poor compensation ability
	IIR filter [126], [141]-[144]	• Simple implementation • Accurate phase compensation	• Noise amplification at high frequency • Relatively complex parameters design
	HPF [94], [139], [140]	• Simple implementation • Ideal derivative characteristics at low frequency	• Over compensation at low frequency • Noise amplification at high frequency
Modified sampling methods	Multiple sampling [95], [107], [145]-[147]	• Reduce delay • Increase the control bandwidth	• Introduce the switching noise and aliasing • Increased computational burden
	Shifting the sampling instant [91], [148]	• Reduce delay • Easy implementation with simple algorithm	• Introduce the switching noises and aliasing • Reduced computational time • Limited by computational speed
	Shifting the update instant of reference voltage [149]	• Reduce delay • Easy implementation with simple algorithm	• Limited by computational speed
	Dual sampling modes [120]	• Eliminate delay completely • Extend the sampling interval • Improve the current control performance • Avoid switching noises	• Complicated algorithm • Computational burden • Unsuitable for three-phase grid-connected inverters

approaches, then is the predictive control schemes. However, the influence of delay on system stability can only be alleviated rather than thoroughly eliminated by applying the modified sampling methods, except for the dual sampling modes. Therefore, a reasonable tradeoff between the implementation complexity and compensation effect could be attained by means of digital filters with phase lead characteristics.

Certainly, by using the delay compensation approaches and various damping methods, the internal stability of individual inverter itself can be improved to the most extent. However, the interactions between the inverter and the grid as well as among paralleled inverters still challenge the external stability of the inverter, thus the corresponding concerns about the external interaction stability of the inverter-grid system are discussed in the forthcoming Section.

IV. IMPEDANCE-BASED METHOD FOR EXTERNAL STABILITY

The external stability of the inverter can be evaluated with the utilization of impedance-based stability criterion. In order to achieve stability assessment, a suitable impedance model of the inverter should be obtained first by employing reasonable modeling methods. Moreover, the grid impedance is supposed to be acquirable through relevant measurement techniques. Meanwhile, the attention is also worth paying to the two types of interaction in the multi-inverter applications by means of impedance-based method.

A. IMPEDANCE-BASED STABILITY CRITERION

The impedance-based stability analysis method is originally presented to analyze the stability of DC systems [150], and then introduced to the investigation of AC systems [39]. The current-controlled inverter-grid system can be separated as an inverter subsystem and a grid subsystem by applying the impedance-based analysis method, in which case the inverter and the grid can be respectively denoted by a current source in parallel with an impedance and a voltage source in series with an impedance [39], as shown in Fig. 15, where $u_g(s)$ is the grid voltage, $u_{pcc}(s)$ is the voltage at PCC, $i_2(s)$ is the injected grid current, and $i_s(s)$ is the ideal current source.

In Fig. 15(a), the equivalent output impedance of the inverter is defined as $Z_o(s)$, the grid impedance $Z_g(s)$ is mainly dependent on the transmission lines and transformer impedances [5]. The injected grid current can be expressed by (17), which indicates that a large value of $Z_o(s)$ represents good steady-state performance [46].

$$i_2(s) = [i_s(s) - \frac{u_g(s)}{Z_o(s)}]\frac{1}{1 + Z_g(s)/Z_o(s)} \tag{17}$$

According to [39], the interconnected inverter-grid system is stable if one of the following conditions is satisfied, which can be implemented by either cancelling the equivalent grid impedance [152] or increasing the inverter output impedance [46].

1) $Z_g(s) = 0$.

2) $Z_g(s)/Z_o(s)$ satisfies the Nyquist stability criterion.

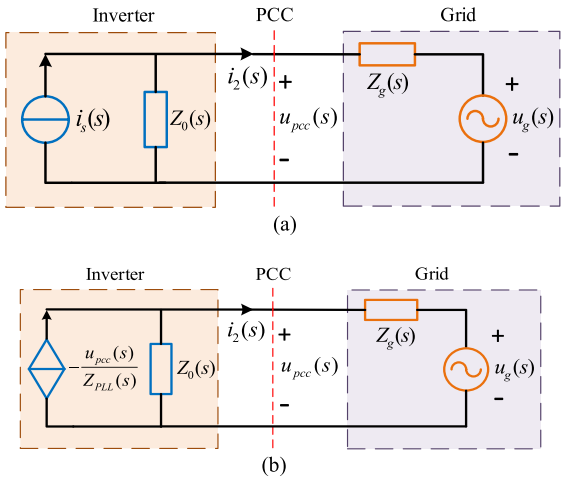

FIGURE 15. Equivalent circuit of the inverter-grid system [39], [151]. (a) When the PLL is neglected. (b) When the PLL is considered.

Furthermore, the inverter can be regarded as a controlled current source in the case of considering the phase-locked loop (PLL), as shown in Fig. 15(b), where $Z_{PLL}(s)$ is the equivalent impedance of PLL which can be found in [151]. In this scenario, the injected grid current can be calculated by (18), and the stability conditions are consistent with that of Fig. 15(a).

$$i_2(s) = -\frac{u_g(s)}{Z_{inv}(s)}\left(\frac{1}{1+Z_g(s)/Z_{inv}(s)}\right) \tag{18}$$

In (18), $Z_{inv}(s)$ is the equivalent output impedance of the inverter, which is the parallel form of $Z_o(s)$ and $Z_{PLL}(s)$.

B. IMPEDANCE MODELING METHODS

In order to implement the impedance-based stability analysis, the inverter output impedance should be obtained in advance. Specifically, according to the relationship between the voltage at PCC and the injected grid current, the impedance model based on the equivalent transfer function can be derived by means of direct linearization in steady state [153]. However, the practical AC systems are nonlinear caused by switching devices and controllers, which can be approximately linearized by applying the conventional small-signal methods. It is worth noting that, the direct small-signal linearization is incapable for time-varying AC systems due to the absence of the fixed steady-state operating point, in which case the variables needs to be denoted in the *dq*-, sequence- or phasor-domains, thereby the small-signal linearization can be executed for modeling and stability analysis [37]. The detailed discussions about the different impedance modeling methods are presented as follows.

1) EQUIVALENT TRANSFER FUNCTIONS

By using the equivalent transformation of the control block diagrams of the system, the inverter output impedance is available in steady state. Concretely, the block diagrams of the transfer functions of system can be equivalently transformed as shown in Fig. 16, and the detailed transformation process can be found in [46].

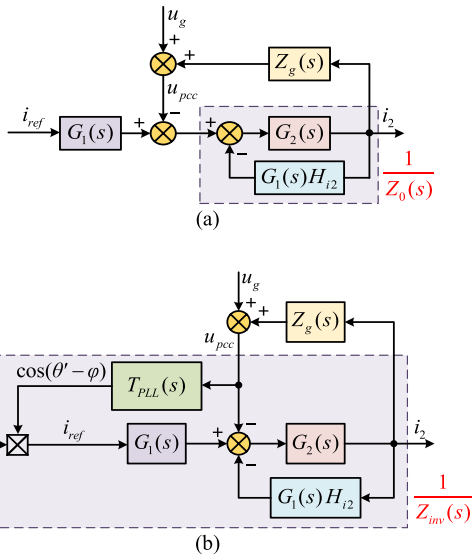

FIGURE 16. The equivalent transfer function block diagrams of the system [46], [151]. (a) When the SRF-PLL is neglected. (b) When the SRF-PLL is considered.

The $G_1(s)$ and $G_2(s)$ are the equivalent terms of the system block diagrams after transformation, which vary with the different damping methods and controller parameters. The H_{i2} is the sensor gain of grid current, I^*_{ref} is the amplitude command of the current reference i_{ref}, $\theta^{'}$ is the extracted voltage phase of PCC by the mostly used synchronous rotating reference-frame PLL (SRF-PLL) [154], φ is the power-factor angle. The phase of i_{ref} is $(\theta^{'} - \varphi)$ since the grid-connected inverter is required to output reactive power. The T_{PLL} is the transfer function model of SRF-PLL which can be found in [151]. In this scenario, the equivalent output impedances of the inverter in Fig. 16 can be respectively derived as follows:

$$Z_o = -\frac{u_{pcc}}{i_2} = \frac{1+G_1G_2H_{i2}}{G_2} \tag{19}$$

$$Z_{inv} = -\frac{u_{pcc}}{i_2} = \frac{1+G_1G_2H_{i2}}{G_2 - I^*_{ref}T_{PLL}G_1G_2} \tag{20}$$

In (20), the equivalent output impedance of the inverter is decreased due to the additional polynomial $-T_{PLL}I^*_{ref}G_1G_2$ introduced by SRF-PLL regardless of the damping methods, which deteriorates the system stability.

In [46], [151], [153], [155]–[157], the feedforward scheme of grid voltage is proposed to reshape the output impedance phase of the inverter at the intersection frequency where the magnitudes of Z_o and Z_g are equal, thereby enlarging the phase margin of the system. However, the system stability is susceptible to the negative phase angle introduced by the feedforward strategy. Fortunately, it can be solved by boosting the phase angle of inverter output impedance with the utilization of improved feedforward strategy [158].

Apart from the single-phase inverter systems, this method can also be applied to the three-phase systems controlled

in $\alpha\beta$ frame since no coupling effect exists between the α- and β-axis components [30].

2) DQ-DOMAIN IMPEDANCE MODELING

The impedance models in dq-domain are easily compatible with each other in an overall system model since most of the three-phase systems are controlled in the dq-frame, without additional transformation [37]. With respect to a three-phase inverter system controlled in dq-frame, the three-phase variables are transformed into two DC quantities, i.e., the d- and q-axis components. In this case, the equivalent output impedance of inverter in dq-domain can be obtained by using the conventional small-signal linearization method around the DC operation points, and each link in the transfer function flow chart is represented by a two-dimensional matrix. Hence, the terminal characteristics of the inverter can be represented by an impedance matrix as follows [48]:

$$Z_{\text{inv}} = \begin{bmatrix} \tilde{v}_d \\ \tilde{v}_q \end{bmatrix} \begin{bmatrix} \tilde{i}_d \\ \tilde{i}_q \end{bmatrix}^{-1} = \begin{bmatrix} Z_{dd} & Z_{dq} \\ Z_{qd} & Z_{qq} \end{bmatrix} \tag{21}$$

where $\tilde{i}_d$ and $\tilde{i}_q$ are the current perturbation signals, $\tilde{v}_d$ and $\tilde{v}_q$ are the corresponding voltage responses, and $\boldsymbol{Z}_{inv}$ is the output impedance matrix of the inverter.

It has demonstrated that, the crossing-coupling impedances Z_{dq} and Z_{qd} can be neglected in the case of unity power factor controlled inverters [159], [160], in which case the system stability can be investigated by applying two single-input and single-output (SISO) models. Moreover, the stability of inverter system is susceptible to the negative incremental resistance Z_{qq} introduced by PLL at low frequency [161]–[164], whereas the negative resistance characteristics are existed in Z_{dd} for rectifier systems [165]. In order to modify the q-axis output impedance Z_{qq} into a positive resistance, a feedforward control strategy of the voltage at PCC is adopted in [166]–[168]. Yet, the inaccurate stability analysis may be caused by the inherent phase drop of the inverter output impedance, which is introduced by the control delay in the feedforward path, and this problem can be solved by means of reduced feedforward gain [49].

It is noteworthy that, several uncertainties in practice, such as the unbalanced three-phase AC systems and the phase tracking error of PLL, may influence the accuracy of stability analysis [169], which needs to be further explored. Moreover, with respect to the d- and q-axis impedances, there is unspecific physical interpretation due to the artificial frame [37]. The d- and q-axis terminals are not physical existing for connecting sensors, and the dq-frame must be processed in real time, which results in inconvenient experimental measurement owing to the special requirements of the measurement algorithms and devices [170].

3) PHASOR-DOMAIN IMPEDANCE MODELING

In phasor-domain, the sinusoidal voltages and currents can be respectively denoted by the phasors composed of two state variables for more accurate system modeling, in which case the phasors are DC quantities in steady state [37]. In [171], a 2×2 phasor-domain impedance matrix is defined by injecting sinusoidal disturbances of real and imaginary parts, which allows the direct linearization of single-phase system for impedance-based stability analysis. Moreover, the terminal characteristics of the inverter can also be described by defining the amplitude perturbation $\tilde{V}_m$ and phase perturbation $\tilde{V}_\theta$ at fundamental frequency [172], expressed as (22).

$$\begin{bmatrix} \tilde{I}_m(s) \\ \tilde{I}_\theta(s) \end{bmatrix} = \begin{bmatrix} Y_{mm}(s) & Y_{m\theta}(s) \\ Y_{\theta m}(s) & Y_{\theta\theta}(s) \end{bmatrix} \begin{bmatrix} \tilde{V}_m(s) \\ \tilde{V}_\theta(s) \end{bmatrix} \tag{22}$$

where $\tilde{I}_m$ and $\tilde{I}_\theta$ are the current responses, and the transfer matrix is the inverter output admittance in phasor domain.

It is worth noting that, the impedance modeling and stability analysis of the inverter in phasor-domain is immature at present, which needs to be further explored.

4) SEQUENCE-DOMAIN IMPEDANCE MODELING

Besides, the harmonic linearization techniques can also be used to derive a linearization model of an inverter along a sinusoidal trajectory [37]. Concretely, by superimposing the sinusoidal voltage perturbations of the positive- and negative-sequences onto the time-varying operating trajectory, the inverter output impedance in sequence-domain can be obtained according to the current responses at the perturbation frequency, which is denoted by an admittance matrix as follows [173]:

$$\begin{bmatrix} \tilde{I}_p(s+j\omega_0) \\ \tilde{I}_n(s-j\omega_0) \end{bmatrix} = \begin{bmatrix} Y_{pp}(s) & Y_{pn}(s) \\ Y_{np}(s) & Y_{nn}(s) \end{bmatrix} \begin{bmatrix} \tilde{V}_p(s+j\omega_0) \\ \tilde{V}_n(s-j\omega_0) \end{bmatrix} \tag{23}$$

where the subscripts p and n represent the positive- and negative-sequence components, respectively, $\tilde{V}$ is the voltage perturbation, $\tilde{I}$ is the current response, and ω_0 is the fundamental angular frequency of grid voltage.

In [174], the sequence impedances are derived by the harmonic linearization techniques without considering the PLL, whereas the inaccurate stability analysis may be caused since the coupling effect between the off-diagonal components of the impedance matrix is neglected, even in balanced three-phase systems [175]. Hence, a modified decoupled sequence impedance [176] and harmonic transfer matrices method [177] are proposed to describe the coupling effect, which are equivalent to the dq-domain impedance model [178]. Moreover, the dq-domain impedance matrix can be converted into two decoupled SISO sequence-domain impedances by regarding the interconnection system as a closed-loop system instead of two subsystems [179], thereby the conventional NSC can be adopted for impedance-based stability analysis.

In order to analyze the merits and drawbacks of the various impedance modeling methods, a comprehensive comparison is conducted in Table 8. Actually, the equivalent transfer functions are SISO models, in which case the inverter systems are regarded as linear and time-invariant (LTI). Hence, the classical gain margin (GM) and phase margin (PM) in Bode diagram can be employed to design the reasonable system

TABLE 8. Merits and drawbacks of the different impedance modeling methods.

Impedance modeling methods	Specific implementation methods	Merits	Drawbacks	Applications
Equivalent transfer functions [46], [151], [153], [155]-[158]	• Transform the transfer function block diagrams equivalently	• Clear physical interpretation for the impedances • Simple implementation • Facilitate parameters design	• Relatively low model accuracy	• Single-phase systems • Balanced three-phase systems controlled in $\alpha\beta$-frame
dq-domain impedance modeling [49], [159]-[169]	• Small-signal linearization in dq-frame • Represent the impedance by 2-demensional matrix	• Three-phase inverters are usually controlled in dq-frame • Compatible with overall system model	• Exist coupling between d- and q-axis components • Cannot measure d- and q-axis components through experiments directly	• Balanced three-phase systems
Phasor-domain impedance modeling [171], [172]	• Represent the state variables with phasors	• Describe the system model accurately	• Immature impedance-based stability analysis	• Single-phase systems • Balanced three-phase systems
Sequence-domain impedance modeling [173]-[179]	• Harmonic linearization and symmetrical component method	• Clear physical interpretation for the impedance models • Impedances can be measured through experimentations directly	• Exist coupling between sequence impedances • Complicated linearization process	• Three-phase systems

parameters, thereby reshaping the equivalent inverter output impedances for improving the system stability. However, the impedance models in dq-, phasor- and sequence-domains are multiple-input and multiple-output (MIMO) transfer matrixes. In this scenario, the system stability should be evaluated by means of generalized Nyquist stability criterion (GNSC) [180], which can be denoted as follows:

$$\boldsymbol{T}(s) = \boldsymbol{Z}_{inv}(s)\boldsymbol{Y}_g(s) \tag{24}$$

where $\boldsymbol{Z}_{inv}(s)$ is the impedance matrix of the inverter, and $\boldsymbol{Y}_g(s)$ is the grid admittance matrix. The eigenvalues $\lambda_1(s)$ and $\lambda_2(s)$ of $\boldsymbol{T}(s)$ are two characteristic locus that vary with the variable s in the complex plane, and the interconnected system is stable if and only if the $(-1, j0)$ is not encircled by the Nyquist curves of $\lambda_1(s)$ and $\lambda_2(s)$. Nevertheless, the GNSC is usually utilized to assess the system stability, and the relevant researches about how to design system parameters according to the assessment results are still insufficient.

Indeed, the analytical inverter output impedance can be acquired by means of aforementioned theoretical derivation. Yet, the impedance model is unavailable due to the missing system parameters in some special cases, which impedes the application of impedance-based stability analysis. Fortunately, the output impedance can also be measured by capturing the terminal characteristics of the inverter through injecting the perturbation signals into the grid voltage [49], in which case the system is regarded as a black box. Moreover, the theoretical derivation method is unsuitable for modeling grid impedance, thus the relative measurement techniques should be adopted. Hence, the signal-injection based impedance measurement techniques are discussed herein.

C. ONLINE IMPEDANCE MEASUREMENT TECHNIQUES

Recently, some studies about the signal-injection-based impedance measurement have been published. By injecting a sinusoidal excitation into the system at the predetermined frequency and capturing the output response at that frequency, the sine sweep technique is applied to calculate the impedance through point-by-point measurement in a specific frequency range with several frequency points [170], [191], which is reliable due to its high signal-to-noise ratio (SNR). However, as for the time-varying grid impedance, the off-line measurement is insufficient for accurate stability analysis. In this scenario, the sine sweep technique is not suitable any more on account of the time-consuming measurement, thus the online impedance measurement methods with short processing time should be adopted for the online stability analysis in real time, thereby reshaping the inverter output impedance adaptively. The injection signals could be the single impulse [51] or the pulse sequences [52], in which case the signal contains abundant harmonics information. Therefore, the grid impedance can be accurately estimated within a period of about one fundamental cycle [51].

As shown in Fig. 17, in these online methods, by injecting a current perturbation on the top of the current reference i_{dref} (i_{qref}) and measuring the voltage responses, the corresponding frequency components in response and perturbation are extracted by means of Fourier analysis, then the grid

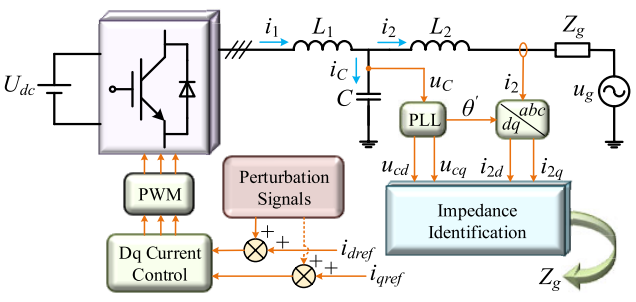

FIGURE 17. Schematic diagram of the online grid impedance identification based on perturbation signals injection [51].

impedance is timely acquired by the ratio between the voltage u_{Cd} (u_{Cq}) and the current $i_{2\,d}$ ($i_{2\,q}$) at different frequencies, without extra sensors and signal generators.

In [181], an impulse current is employed to measure online grid impedance, thus regulating the inverter output impedance accordingly. Nevertheless, the normal operation of the system may be affected by the large impulse amplitude. In [183] and [184], the single impulse is replaced by the maximum-length binary sequences (MLBS) with lower time-domain amplitude to estimate the grid impedance. Subsequently, the parameters of PLL and grid-voltage feedforward are correspondingly adjusted to adapt the *dq*-domain impedance of the inverter, respectively. Yet, the MLBS are insufficient for impedance identification under strong grid conditions due to the distributed power of the signal in the wide frequency range, thus the discrete-interval binary sequences (DIBS) based on several specified harmonic frequencies are applied in [185] and [186] to increase the energy of the signals, without enlarging the signal amplitude. However, the methods using MLBS and DIBS are time consuming and inaccurate owing to the possible variation of operating conditions during the experiments, since the perturbation signals are separately injected into the *d*- and *q*-components of current reference. Hence, the orthogonal pseudo-random binary sequences (OPRBS) are adopted in [187]–[189] to identify the *d*- and *q*-axis impedance components simultaneously during a single measurement cycle, with reduced measurement time and improved estimation accuracy.

Actually, the MLBS, DIBS and OPRBS are the pseudo-random binary sequences (PRBS), which have levels of -1 and $+1$. It is noteworthy that, the nonlinearities of the inverter may degrade the measurement accuracy when the impulse and PRBS are used, since the controller design is usually based on the linear model [190]. Therefore, in order to eliminate the estimation errors caused by nonlinear factors, only the linear components of the grid impedance are identified in [190] by using the ternary sequences, in which case the levels of the ternary sequences are -1, 0 and $+1$.

Specifically, the advantages and disadvantages of various measurement techniques are summarized in Table 9. In conclusion, the processing time of single impulse injection is shorter than the binary and ternary sequences injection methods, whereas the latter two approaches are more reliable in view of the system stability due to the smaller time-domain amplitudes. Hence, the pulse sequences are suitable for the perturbed sensitive systems. As for the selection of the perturbation signals, it is worth noting that the signal amplitude should be carefully determined, since a large amplitude may interfere with the normal operation of the system, yet a small amplitude is deficient for impedance measurement due to the low SNR [51]. Another consideration is the generation frequency of the sequences, a high value of frequency is advantageous to provide enough energy for the sequences [190], yet a low value, below one-third of the sampling frequency of the inverter, contributes to achieve precise measurement [192].

D. STABILITY ANALYSIS OF MULTI-PARALLELED GRID-CONNECTED INVERTERS

The multi-paralleled inverters are increasingly employed to enlarge the total generation capacity in recent years. In this scenario, apart from the interaction between the grid and the inverter, the additional interaction instability among inverters may also arise as the number of inverters increases [193]. In [194] and [195], an innovative interaction analysis method based on the current separation scheme is proposed, which divides each inverter output current into the interactive current circulated among the paralleled inverters and the common current injected to the grid. It is revealed that, the stability of two current components can be individually evaluated by two independent SISO model.

However, the current separation expression in [194] is non-intuitive and complicated for the system-level stability analysis of paralleled inverters, in which case the impedance-based method can be easily extended and modularized for the modeling and stability analysis of the system. The Norton equivalent circuits of multiple paralleled inverters in Fig. 18(a), thus, are established in [29], which imparts that both two types of interaction in the parallel system would cause the distorted grid current. Specifically, the interaction among inverters is mainly caused by the change of current references of other inverters, such as in a PV plant where the current references are generally varied in every several seconds, and the interaction between the grid and the inverter is induced by the grid voltage harmonics and transient disturbances [29]. Further, in order to simplify the system model, an equivalent inverter is adopted in [27] to model *n* paralleled equal inverters, which reveals the impedance multiplication effect, i.e., the equivalent grid impedance is *n* times the original value, as shown in Fig. 18(b). In this case, the stability of the inverters-grid system is worsened due to the *n* times grid impedance.

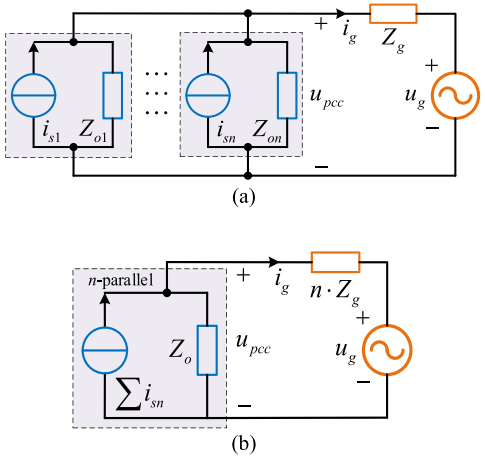

FIGURE 18. (a) Equivalent circuit of *n*-parallel inverters. (b) Simplified equivalent circuit of n-parallel inverters [196].

Nevertheless, the above analysis is ideally implemented with the hypothesis of identical paralleled inverters, and the more general scenarios should be taken into account. In [197],

TABLE 9. Advantage and disadvantages of the online impedance measurement techniques.

Injected signals	Advantages	Disadvantages	Applications
Single impulse [51], [181], [182]	• Simple implementation • Insensitive to the no-stationary nature of AC systems • Short testing time	• May interfere with the normal operation of the inverter • Relatively low measurement accuracy	• Insensitive systems for perturbations • Weak grid
MLBS [52], [183], [184]	• Small excitation amplitude • Simple implementation • Easy data acquisition	• Neglect the crossing-coupling effect between the impedance components • Cannot measure the impedance components in the same operation conditions • Energy is distributed over many harmonic frequencies	• Sensitive systems for perturbations • Balanced three-phase systems • Weak grid
DIBS [185], [186]	• Small excitation amplitude • Simple implementation • Easy data acquisition • Maximize the energy of the signals	• Neglect the crossing-coupling effect between the impedance components • Cannot measure the impedance components in the same operation conditions	• Balanced three-phase systems • Strong grid
OPRBS [187]-[189]	• Save the test time • Measure each impedance component in the same operation conditions	• Neglect the crossing-coupling effect between the impedance components • Sequence lengths are different	• Balanced three-phase systems • Weak grid
Ternary sequence [190]	• Much wider of the sequence length • More efficient • Minimize the effect of nonlinearities	• Neglect the crossing-coupling effect between the impedance components • Cannot measure the impedance components in the same operation conditions	• Balanced three-phase systems • Weak grid

the multiplication effect is extended when the power ratings and line impedances of the paralleled inverters are different with each other, and the stability contributions corresponding to inverters are analyzed. Furthermore, the interaction stability containing the inverters with various control structures is explored in [198], which indicates that the interactive instability among inverters would arise if the inverters have common right-half-plane (RHP) poles, and the interconnected system is stable if the admittance network defined in [198] is stable. Also, the overall stability of the system composed of current- and voltage-controlled inverters is predicted in [199] by means of inverter output impedances. In addition, as for the offshore paralleled inverters, the impedance model of whole system is revised in [200] with the consideration of the differences among the inverters and the long cables, in which case a long cable is equivalent to a decoupling two-port circuit model. It is worth noting that, most of the existing researches only focus on the modeling and stability analysis of multi-paralleled inverters system, and the design guidance of overall system based on the interaction analysis results, similar to the design procedure in [201], is still immature. Moreover, from the perspective of impedance model, the study on the contribution of each inverter to the overall system stability is also insufficient.

Additionally, in order to enhance the interaction stability, the inverter output impedances are enlarged by means of grid voltage feedforward in [196], and it is claimed that increasing the inverter output impedances is the only effective method to enhance the interaction stability between the grid and the inverter in the low frequency range. Instead of reshaping the inverter output impedances, an active power filter (APF) is installed at the PCC to adjust the equivalent grid impedance in [202], thereby improving the interaction stability. Similarly, the above approaches are ideally achieved since the paralleled inverters are regarded as identical with each other.

V. CONCLUSION AND FUTURE WORK

This paper presents a comprehensive overview of the state-of-the-art techniques on the *LCL*-type grid-connected inverters, including the *LCL*-filter design, the damping methods for improving the internal stability of individual inverter, and the impedance-based analysis method for assessing the system-level external stability of inverter-grid system.

Firstly, the parameters of the *LCL* filter should be meticulously selected according to the design constraints to achieve the desired filtering performance, so that improves the quality of injected grid current for avoiding the grid oscillation or even destabilization caused by harmonics pollution. The specific parameters to be designed include the filter capacitor, the total inductance, the inverter-side inductance, the harmonic attenuation rate and the resonance frequency. Further, by applying the magnetic integration techniques, the size and weight of the bulky inductors in conventional filters can be diminished to increase the power density of the system.

In order to maintain the internal stability of *LCL*-type grid-connected inverters, the filter- and state-feedback-based damping methods are preferred to suppress the inherent *LCL*-filter resonance peak, with the advantages of flexibility, efficiency and zero power loss. In comparison, the filter-based damping methods are low cost and simple implementation, whereas the state-feedback-based methods are more robust in the case of grid impedance variation. Yet, the digital control delay has significant effects on the two damping methods. Generally, the extra countermeasures should be adopted to eliminate the impacts of delay on the system stability, such as the predictive control techniques, filter-based compensation methods and modified sampling approaches.

As for the external stability at the system level, the impedance-based analysis method is prevalent for

predicting the external instability induced by the interactive resonances between the inverter and the weak grid as well as among inverters, especially in the multi-paralleled inverters system. The SISO equivalent transfer functions are suitable for modeling the single-phase and balanced three-phase system controlled in stationary frame. The MIMO transfer matrixes can be utilized to describe the inverter output impedances in *dq*-, phasor- and sequence-domains, in which case the GNSC should be applied to study the system stability. The inverter output impedances can also be measured by perturbation injection methods with short measurement time, such as the single impulse current and pulse current sequences, and the measurement techniques are also applicable for identifying the grid impedance in real time. Moreover, the unstable interaction between the inverter and the grid can be settled by reducing the PLL bandwidth, employing the grid voltage feedforward scheme or installing an APF at PCC.

Finally, the future research trends of the *LCL*-type grid-connected inverters are summarized as follows:

1) With respect to the magnetic integration techniques applied in the *LCL*-filter design, these methods can also be adopted to construct equivalent multi-branch filters by fully utilizing the mutual inductances between the integrated inductors, in which case the filters have the strong harmonic attenuation capability at the selected frequency and high power density, with the cost and weight as low as possible.
2) Theoretically, the adverse impacts of control delay on the CCF-based damping methods can be fully eliminated by using the predictive control techniques. However, the reduction of computation burden and the immunity of prediction to the system parameters variation needs to be further improved for high-order systems. Moreover, the control parameters of the various damping methods are supposed to be adaptively tuned online to strengthen the system robustness in the case of applying the high-speed processors and superior model prediction algorithms.
3) Currently, the PWM inverter is generally regarded as a linear and balanced system to model its output impedance, whereas the unbalanced characteristics and the several nonlinear factors, such as dead time and PLL, may result in imprecise stability analysis. Furthermore, the lack of simple and applicable stability indexes, similar to the gain and phase margins, impedes the further application of impedance-base stability analysis for systematic control design and parameters tuning.
4) Most of the existing online grid impedance measurement techniques are insufficient, since only the balanced three-phase systems are normally considered and the crossing-coupling effect between the non-diagonal components in the impedance matrix are neglected. It is worth noting that, the essence of the online measurement techniques is to determine the impedance values according to the ratios between perturbation signals and the resulting responses, thus the effect of these small disturbances on the system stability should be evaluated in detail. Concretely, how to achieve an appropriate tradeoff between the system stability and the effective measurement, there is no quantitative selection principle for the amplitude of the perturbation signal, which is usually chosen base on the experience of designers.
5) From the perspective of impedance stability analysis, the contribution of individual inverter to overall system stability in a multi-paralleled inverters application and the identification of the dominant unstable subsystems should be further explored. Furthermore, according to the stability contribution of each inverter, the reasonable impedance sharing control among paralleled inverters is worth considering, in order to maintain the interaction stability among inverters as well as between the inverters and the grid. In addition, the practical multi-paralleled inverters are not completely identical, thus the more general scenarios containing different inverters need to be further studied, such as the differences in power ratings and transmission lines and various types of inverters.

REFERENCES

[1] F. Blaabjerg, R. Teodorescu, M. Liserre, and A. V. Timbus, "Overview of control and grid synchronization for distributed power generation systems," *IEEE Trans. Ind. Electron.*, vol. 53, no. 5, pp. 1398–1409, Oct. 2006.
[2] A. Timbus, M. Liserre, R. Teodorescu, P. Rodriguez, and F. Blaabjerg, "Evaluation of current controllers for distributed power generation systems," *IEEE Trans. Power Electron.*, vol. 24, no. 3, pp. 654–664, Mar. 2009.
[3] M. A. Eltawil and Z. Zhao, "Grid-connected photovoltaic power systems: Technical and potential problems—A review," *Renew. Sustain. Energy Rev.*, vol. 14, no. 1, pp. 112–129, Jan. 2010.
[4] I. J. Balaguer, Q. Lei, S. Yang, U. Supatti, and F. Z. Peng, "Control for grid-connected and intentional islanding operations of distributed power generation," *IEEE Trans. Ind. Electron.*, vol. 58, no. 1, pp. 147–157, Jan. 2011.
[5] W. Wu, Y. Liu, Y. He, H. S.-H. Chung, M. Liserre, and F. Blaabjerg, "Damping methods for resonances caused by LCL-filter-based current-controlled grid-tied power inverters: An overview," *IEEE Trans. Ind. Electron.*, vol. 64, no. 9, pp. 7402–7413, Sep. 2017.
[6] H. Cha and T.-K. Vu, "Comparative analysis of low-pass output filter for single-phase grid-connected Photovoltaic inverter," in *Proc. IEEE Appl. Power Electron. Conf. Expo. (APEC)*, Feb. 2010, pp. 1659–1665.
[7] M. Büyük, A. Tan, M. Tümay, and K. Ç. Bayindir, "Topologies, generalized designs, passive and active damping methods of switching ripple filters for voltage source inverter: A comprehensive review," *Renew. Sustain. Energy Rev.*, vol. 62, pp. 46–69, Sep. 2016.
[8] S. Ponnaluri, V. Krishnamurthy, and V. Kanetkar, "Generalized system design and analysis of PWM based power electronic converters," in *Proc. IEEE Ind. Appl. Conf.*, Oct. 2000, pp. 1972–1979.
[9] V. Blasko and V. Kaura, "A novel control to actively damp resonance in input *LC* filter of a three-phase voltage source converter," *IEEE Trans. Ind. Appl.*, vol. 33, no. 2, pp. 542–550, Mar. 1997.
[10] Y. W. Li, "Control and resonance damping of voltage-source and current-source converters with *LC* filters," *IEEE Trans. Ind. Electron.*, vol. 56, no. 5, pp. 1511–1521, May 2009.
[11] E. Twining and D. G. Holmes, "Grid current regulation of a three-phase voltage source inverter with an LCL input filter," *IEEE Trans. Power Electron.*, vol. 18, no. 3, pp. 888–895, May 2003.
[12] J. Dannehl, C. Wessels, and F. W. Fuchs, "Limitations of voltage-oriented PI current control of grid-connected PWM rectifiers with *LCL* filters," *IEEE Trans. Ind. Electron.*, vol. 56, no. 2, pp. 380–388, Feb. 2009.

[13] C. Bao, X. Ruan, X. Wang, W. Li, D. Pan, and K. Weng, "Step-by-step controller design for LCL-type grid-connected inverter with capacitor–current-feedback active-damping," *IEEE Trans. Power Electron.*, vol. 29, no. 3, pp. 1239–1253, Mar. 2014.
[14] Y. Liu, W. Wu, Y. He, Z. Lin, F. Blaabjerg, and H. S.-H. Chung, "An efficient and robust hybrid damper for *LCL* or *LLCL*-based grid-tied inverter with strong grid-side harmonic voltage effect rejection," *IEEE Trans. Ind. Electron.*, vol. 63, no. 2, pp. 926–936, Feb. 2016.
[15] X. Li, J. Fang, Y. Tang, and X. Wu, "Robust design of LCL filters for single-current-loop-controlled grid-connected power converters with unit PCC voltage feedforward," *IEEE J. Emerg. Sel. Top. Power Electron.*, vol. 6, no. 1, pp. 54–72, Mar. 2018.
[16] M. H. Mahlooji, H. R. Mohammadi, and M. Rahimi, "A review on modeling and control of grid-connected photovoltaic inverters with LCL filter," *Renew. Sustain. Energy Rev.*, vol. 81, pp. 563–578, Jan. 2018.
[17] J. Xu and S. Xie, "LCL-resonance damping strategies for grid-connected inverters with LCL filters: A comprehensive review," *J. Modern Power Syst. Clean Energy*, vol. 6, no. 2, pp. 292–305, Mar. 2018.
[18] M. Liserre, F. Blaabjerg, and S. Hansen, "Design and control of an LCL-filter-based three-phase active rectifier," *IEEE Trans. Ind. Appl.*, vol. 41, no. 5, pp. 1281–1291, Sep./Oct. 2005.
[19] K. Jalili and S. Bernet, "Design of *LCL* filters of active-front-end two-level voltage-source converters," *IEEE Trans. Ind. Electron.*, vol. 56, no. 5, pp. 1674–1689, May 2009.
[20] S. Jayalath and M. Hanif, "An LCL-filter design with optimum total inductance and capacitance," *IEEE Trans. Power Electron.*, vol. 33, no. 8, pp. 6687–6698, Aug. 2018.
[21] J. Xu, S. Xie, L. Huang, and L. Ji, "Design of LCL-filter considering the control impact for grid-connected inverter with one current feedback only," *IET Power Electron.*, vol. 10, no. 11, pp. 1324–1332, Sep. 2017.
[22] T.-F. Wu, M. Misra, L.-C. Lin, and C.-W. Hsu, "An improved resonant frequency based systematic LCL filter design method for grid-connected inverter," *IEEE Trans. Ind. Electron.*, vol. 64, no. 8, pp. 6412–6421, Aug. 2017.
[23] C. Poongothai and K. Vasudevan, "Design of LCL filter for grid-interfaced PV system based on cost minimization," *IEEE Trans. Ind. Appl.*, vol. 55, no. 1, pp. 584–592, Jan./Fed. 2019.
[24] Y. Liu, K. Y. See, K. J. Tseng, R. Simanjorang, and J.-S. Lai, "Magnetic integration of three-phase LCL filter with delta-yoke composite core," *IEEE Trans. Power Electron.*, vol. 32, no. 5, pp. 3835–3843, May 2017.
[25] J. Fang, X. Li, X. Yang, and Y. Tang, "An integrated trap-LCL filter with reduced current harmonics for grid-connected converters under weak grid conditions," *IEEE Trans. Power Electron.*, vol. 32, no. 11, pp. 8446–8457, Nov. 2017.
[26] X. Li, P. Lin, and Y. Tang, "Magnetic integration of LTL filter with two LC-traps for grid-connected power converters," *IEEE J. Emerg. Sel. Topics Power Electron.*, vol. 6, no. 3, pp. 1434–1446, Sep. 2018.
[27] J. L. Agorreta, M. Borrega, J. López, and L. Marroyo, "Modeling and control of N-paralleled grid-connected inverters with LCL filter coupled due to grid impedance in PV plants," *IEEE Trans. Power Electron.*, vol. 26, no. 3, pp. 770–785, Nov. 2011.
[28] H.-C. Chen, P.-T. Cheng, F. Blaabjerg, and X. Wang, "A passivity-based stability analysis of the active damping technique in the offshore wind farm applications," *IEEE Trans. Ind. Appl.*, vol. 54, no. 5, pp. 5074–5082, Sep./Oct. 2018.
[29] J. He, Y. W. Li, D. Bosnjak, and B. Harris, "Investigation and active damping of multiple resonances in a parallel-inverter-based microgrid," *IEEE Trans. Power Electron.*, vol. 28, no. 1, pp. 234–246, Jan. 2013.
[30] X. Ruan, X. Wang, D. Pan, D. Yang, W. Li, and C. Bao, *Control Techniques for LCL-Type Grid-Connected Inverters*. Singapore: Springer, 2017.
[31] R. N. Beres, X. Wang, M. Liserre, F. Blaabjerg, and C. L. Bak, "A review of passive power filters for three-phase grid-connected voltage-source converters," *IEEE Trans. J. Emerg. Sel. Topics Power Electron.*, vol. 4, no. 1, pp. 54–69, Mar. 2016.
[32] C. C. Gomes, A. F. Cupertino, and H. A. Pereira, "Damping techniques for grid-connected voltage source converters based on LCL filter: An overview," *Renew. Sustain. Energy Rev.*, vol. 81, pp. 116–135, Jan. 2018.
[33] J. Dannehl, M. Liserre, and F. W. Fuchs, "Filter-based active damping of voltage source converters with *LCL* filter," *IEEE Trans. Ind. Electron.*, vol. 58, no. 8, pp. 3623–3633, Aug. 2011.
[34] P. A. Dahono, "A control method to damp oscillation in the input LC filter," in *Proc. IEEE Annu. Power Electron. Spec. Conf. (PESC)*, vol. 4, Jun. 2002, pp. 1630–1635.
[35] T. Liu, Z. Liu, J. Liu, Y. Tu, and Z. Liu, "Comprehensive analysis of virtual impedance-based active damping for LCL resonance in grid-connected inverters," in *Proc. Int. Power Electron. Conf. (IPEC-ECCE Asia)*, May 2018, pp. 2681–2687.
[36] T. Liu, J. Liu, Z. Liu, and Z. Liu, "A study of virtual resistor-based active damping alternatives for LCL resonance in grid-connected voltage source inverters," *IEEE Trans. Power Electron.*, to be published. doi: 10.1109/TPEL.2019.2911163.
[37] J. Sun, "Small-signal methods for AC distributed power systems—A review," *IEEE Trans. Power Electron.*, vol. 24, no. 11, pp. 2545–2554, Nov. 2009.
[38] Y. Wang, X. Wang, Z. Chen, and F. Blaabjerg, "Small-signal stability analysis of inverter-fed power systems using component connection method," *IEEE Trans. Smart Grid*, vol. 9, no. 5, pp. 5301–5310, Sep. 2018.
[39] J. Sun, "Impedance-based stability criterion for grid-connected inverters," *IEEE Trans. Power Electron.*, vol. 26, no. 11, pp. 3075–3078, Nov. 2011.
[40] Z. Liu, J. Liu, W. Bao, and Y. Zhao, "Infinity-norm of impedance-based stability criterion for three-phase AC distributed power systems with constant power loads," *IEEE Trans. Power Electron.*, vol. 30, no. 6, pp. 3030–3043, Jun. 2015.
[41] Y. Cho, K. Hur, Y. C. Kang, and E. Muljadi, "Impedance-based stability analysis in grid interconnection impact study owing to the increased adoption of converter-interfaced generators," *Energies*, vol. 10, no. 9, p. 1355, Sep. 2017.
[42] X. Wang, L. Harnefors, and F. Blaabjerg, "Unified impedance model of grid-connected voltage-source converters," *IEEE Trans. Power Electron.*, vol. 33, no. 2, pp. 1775–1787, Feb. 2018.
[43] Z. Shuai, Y. Li, W. Wu, C. Tu, A. Luo, and J. Z. Shen, "Divided DQ small-signal model: A new perspective for the stability analysis of three-phase grid-tied inverters," *IEEE Trans. Ind. Electron.*, vol. 66, no. 8, pp. 6493–6504, Aug. 2019.
[44] C. Zhang, M. Molinas, A. Rygg, and X. Cai, "Impedance-based analysis of interconnected power electronics systems: Impedance network modeling and comparative studies of stability criteria," *IEEE J. Emerg. Sel. Topics Power Electron.*, to be published. doi: 10.1109/JESTPE.2019.2914560.
[45] W. Wu, L. Zhou, Y. Chen, A. Luo, Y. Dong, X. Zhou, Q. Xu, L. Yang, and J. M. Guerrero, "Sequence-impedance-based stability comparison between VSGs and traditional grid-connected inverters," *IEEE Trans. Power Electron.*, vol. 34, no. 1, pp. 46–52, Jan. 2019.
[46] X. Wang, X. Ruan, S. Liu, and C. K. Tse, "Full feedforward of grid voltage for grid-connected inverter with LCL filter to suppress current distortion due to grid voltage harmonics," *IEEE Trans. Power Electron.*, vol. 25, no. 12, pp. 3119–3127, Dec. 2010.
[47] X. Wang, F. Blaabjerg, and P. C. Loh, "Passivity-based stability analysis and damping injection for multiparalleled VSCs with LCL filters," *IEEE Trans. Power Electron.*, vol. 32, no. 11, pp. 8922–8935, Nov. 2017.
[48] L. Harnefors, M. Bongiorno, and S. Lundberg, "Input-admittance calculation and shaping for controlled voltage-source converters," *IEEE Trans. Ind. Electron.*, vol. 54, no. 6, pp. 3323–3334, Dec. 2007.
[49] T. Messo, R. Luhtala, A. Aapro, and T. Roinila, "Accurate impedance model of grid-connected inverter for small-signal stability assessment in high-impedance grids," in *Proc. Int. Power Electron. Conf. (IPEC-ECCE Asia)*, May 2018, pp. 3156–3163.
[50] K. Godfrey, *Perturbation Signals for System Identification*. Englewood Cliffs, NJ, USA: Prentice-Hall, 1993.
[51] M. Céspedes and J. Sun, "Online grid impedance identification for adaptive control of grid-connected inverters," in *Proc. IEEE Energy Convers. Congr. Expo. (ECCE)*, Sep. 2012, pp. 914–921.
[52] T. Roinila, M. Vilkko, and J. Sun, "Broadband methods for online grid impedance measurement," in *Proc. IEEE Energy Convers. Congr. Expo. (ECCE)*, Sep. 2013, pp. 3003–3010.
[53] S. Jayalath and M. Hanif, "Generalized LCL-filter design algorithm for grid-connected voltage-source inverter," *IEEE Trans. Ind. Electron.*, vol. 64, no. 3, pp. 1905–1915, Mar. 2017.
[54] Y. Tang, W. Yao, P. C. Loh, and F. Blaabjerg, "Design of LCL filters with LCL resonance frequencies beyond the Nyquist frequency for grid-connected converters," *IEEE Trans. Emerg. Sel. Topics Power Electron.*, vol. 4, no. 1, pp. 3–14, Mar. 2016.
[55] A. A. Rockhill, M. Liserre, R. Teodorescu, and P. Rodriguez, "Grid-filter design for a multimegawatt medium-voltage voltage-source inverter," *IEEE Trans. Ind. Electron.*, vol. 58, no. 4, pp. 1205–1217, Apr. 2011.

[56] T. C. Y. Wang, Z. Ye, G. Sinha, and X. Yuan, "Output filter design for a grid-interconnected three-phase inverter," in *Proc. IEEE Aunu. Power Electron. Spec. Conf. (PESC)*, Jun. 2003, pp. 779–784.

[57] R. Peña-Alzola, M. Liserre, F. Blaabjerg, M. Ordonez, and Y. Yang, "LCL-filter design for robust active damping in grid-connected converters," *IEEE Trans. Ind. Informat.*, vol. 10, no. 4, pp. 2192–2203, Nov. 2014.

[58] M. B. Saïd-Romdhane, M. W. Naouar, I. S. Belkhodja, and E. Monmasson, "Simple and systematic *LCL* filter design for three-phase grid-connected power converters," *Mathematics Comput. Simul.*, vol. 130, pp. 181–193, Dec. 2016.

[59] A. Reznik, M. G. Simões, A. Al-Durra, and S. M. Muyeen, "*LCL* filter design and performance analysis for grid-interconnected systems," *IEEE Trans. Ind. Appl.*, vol. 50, no. 2, pp. 1225–1232, Mar./Apr. 2014.

[60] M. Liserre, F. Blaabjerg, and A. Dell'Aquila, "Step-by-step design procedure for a grid-connected three-phase PWM voltage source converter," *Int. J. Electron.*, vol. 91, no. 8, pp. 445–460, Aug. 2004.

[61] A. Kouchaki and M. Nymand, "Analytical design of passive LCL filter for three-phase two-level power factor correction rectifiers," *IEEE Trans. Power Electron.*, vol. 33, no. 4, pp. 3012–3022, Apr. 2018.

[62] D. G. Holmes and T. A. Lipo, *Pulse Width Modulation for Power Converters: Principles and Practice*. New York, NY, USA: Wiley, 2003.

[63] Y. Jiao and F. C. Lee, "LCL filter design and inductor current ripple analysis for a three-level NPC grid interface converter," *IEEE Trans. Power Electron.*, vol. 30, no. 9, pp. 4659–4668, Sep. 2015.

[64] M. B. Said-Romdhane, M. W. Naouar, I. S. Belkhodja, and E. Monmasson, "An improved LCL filter design in order to ensure stability without damping and despite large grid impedance variations," *Energies*, vol. 10, no. 3, p. 336, Mar. 2017.

[65] J. Fang, H. Li, and Y. Tang, "A magnetic integrated *LLCL* filter for grid-connected voltage-source converters," *IEEE Trans. Power Electron.*, vol. 32, no. 3, pp. 1725–1730, Mar. 2017.

[66] W. G. Hurley and W. H. Wölfle, *Transformers and Inductors for Power Electronics: Theory, Design and Applications*. Chichester, U.K.: Wiley, 2013.

[67] Y. Liu, H. A. Mantooth, J. C. Balda, and C. Farnell, "A variable inductor based *LCL* filter for large-scale microgrid application," *IEEE Trans. Power Electron.*, vol. 33, no. 9, pp. 7338–7348, Sep. 2018.

[68] T.-F. Wu, M. Misra, Y.-Y. Jhang, Y.-H. Huang, and L.-C. Lin, "Direct digital control of single-phase grid-connected inverters with LCL filter based on inductance estimation model," *IEEE Trans. Power Electron.*, vol. 34, no. 2, pp. 1851–1862, Feb. 2019.

[69] D. Pan, X. Ruan, C. Bao, W. Li, and X. Wang, "Magnetic integration of the *LCL* filter in grid-connected inverters," *IEEE Trans. Power Electron.*, vol. 29, no. 4, pp. 1573–1578, Apr. 2014.

[70] K.-J. Lee, N.-J. Park, R.-Y. Kim, D.-H. Ha, and D.-S. Hyun, "Design of an LCL filter employing a symmetric geometry and its control in grid-connected inverter applications," in *Proc. IEEE Power Electron. Spec. Conf. (PESC)*, Jun. 2008, pp. 963–966.

[71] X. Li, J. Fang, P. Lin, and Y. Tang, "Active magnetic decoupling for improving the performance of integrated *LCL*-filters in grid-connected converters," *IEEE Trans. Ind. Electron.*, vol. 65, no. 2, pp. 1367–1376, Feb. 2018.

[72] A. Van Den Bossche and V. C. Valchev, *Inductors and Transformers for Power Electronics*, Boca Raton, FL, USA: CRC Press, 2005.

[73] X.-Q. Guo, W.-Y. Wu, and H.-R. Gu, "Modeling and simulation of direct output current control for *LCL*-interfaced grid-connected inverters with parallel passive damping," *Simul. Model. Pract. Theory*, vol. 18, no. 7, pp. 946–956, Aug. 2010.

[74] R. Peña-Alzola, M. Liserre, F. Blaabjerg, R. Sebastián, J. Dannehl, and F. W. Fuchs, "Analysis of the passive damping losses in *LCL*-filter-based grid converters," *IEEE Trans. Power Electron.*, vol. 28, no. 6, pp. 2642–2646, Jun. 2013.

[75] A. K. Balasubramanian and V. John, "Analysis and design of split-capacitor resistiveinductive passive damping for LCL filters in grid-connected inverters," *IET Power Electron.*, vol. 6, no. 9, pp. 1822–1832, Nov. 2013.

[76] R. N. Beres, X. Wang, F. Blaabjerg, M. Liserre, and C. L. Bak, "Optimal design of high-order passive-damped filters for grid-connected applications," *IEEE Trans. Power Electron.*, vol. 31, no. 4, pp. 2083–2098, Mar. 2016.

[77] P. Channegowda and V. John, "Filter optimization for grid interactive voltage source inverters," *IEEE Trans. Ind. Electron.*, vol. 57, no. 12, pp. 4106–4114, Dec. 2010.

[78] C. Liu, K. Dai, K. Duan, and Y. Kang, "Application of a C-type filter based LCFL output filter to shunt active power filters," *J. Power Electron.*, vol. 13, no. 6, pp. 1058–1069, Nov. 2013.

[79] W. Yao, Y. Yang, X. Zhang, F. Blaabjerg, and P. C. Loh, "Design and analysis of robust active damping for *LCL* filters using digital notch filters," *IEEE Trans. Power Electron.*, vol. 32, no. 3, pp. 2360–2375, Mar. 2017.

[80] R. Peña-Alzola, M. Liserre, F. Blaabjerg, M. Ordonez, and T. Kerekes, "A self-commissioning notch filter for active damping in a three-phase LCL-filter-based grid-tie converter," *IEEE Trans. Power Electron.*, vol. 29, no. 12, pp. 6754–6761, Dec. 2014.

[81] M. Liserre, A. Dell'Aquila, and F. Blaabjerg, "Genetic algorithm-based design of the active damping for an LCL-filter three-phase active rectifier," *IEEE Trans. Power Electron.*, vol. 19, no. 1, pp. 76–86, Jan. 2004.

[82] W. Yao, Y. Yang, X. Zhang, and F. Blaabjerg, "Digital notch filter based active damping for LCL filters," in *Proc. IEEE Appl. Power Electron. Conf. Expo. (APEC)*, Mar. 2015, pp. 2399–2406.

[83] L. Yang, Y. Chen, A. Luo, and K. Huai, "Stability enhancement for parallel grid-connected inverters by improved notch filter," *IEEE Access*, vol. 7, pp. 65667–65678, 2019.

[84] R. Peña-Alzola, J. Roldán-Pérez, E. Bueno, F. Huerta, D. Campos-Gaona, M. Liserre, and G. Burt, "Robust active damping in LCL-filter-based medium-voltage parallel grid inverters for wind turbines," *IEEE Trans. Power Electron.*, vol. 33, no. 12, pp. 10846–10857, Dec. 2018.

[85] J. Roldán-Pérez, E. J. Bueno, R. Peña-Alzola, and A. Rodríguez-Cabero, "All-pass-filter-based active damping for VSCs with LCL filters connected to weak grids," *IEEE Trans. Power Electron.*, vol. 33, no. 11, pp. 9890–9901, Nov. 2018.

[86] W. Wu, Y. He, T. Tang, and F. Blaabjerg, "A new design method for the passive damped LCL and LLCL filter-based single-phase grid-tied inverter," *IEEE Trans. Ind. Electron.*, vol. 60, no. 10, pp. 4339–4350, Oct. 2013.

[87] T. Midtsund, J. A. Suul, and T. Undeland, "Evaluation of current controller performance and stability for voltage source converters connected to a weak grid," in *Proc. IEEE Int. Symp. Power Electron. Distrib. Gener. Syst. (PEDG)*, Jun. 2010, pp. 382–388.

[88] C. Zou, B. Liu, S. Duan, and R. Li, "Stationary frame equivalent model of proportional-integral controller in DQ synchronous frame," *IEEE Trans. Power Electron.*, vol. 29, no. 9, pp. 4461–4465, Sep. 2014.

[89] D. Pan, X. Ruan, and X. Wang, "Direct realization of digital differentiators in discrete domain for active damping of LCL-type grid-connected inverter," *IEEE Trans. Power Electron.*, vol. 33, no. 10, pp. 8461–8473, Oct. 2018.

[90] J. Dannehl, F. W. Fuchs, S. Hansen, and P. B. Thøgersen, "Investigation of active damping approaches for PI-based current control of grid-connected pulse width modulation converters with LCL filters," *IEEE Trans. Ind. Appl.*, vol. 46, no. 4, pp. 1509–1517, Jul./Aug. 2010.

[91] D. Pan, X. Ruan, C. Bao, W. Li, and X. Wang, "Capacitor-current-feedback active damping with reduced computation delay for improving robustness of LCL-type grid-connected inverter," *IEEE Trans. Power Electron.*, vol. 29, no. 7, pp. 3414–3427, Jul. 2014.

[92] X. Wang, C. Bao, X. Ruan, W. Li, and D. Pan, "Design considerations of digitally controlled *LCL*-filtered inverter with capacitor- current-feedback active damping," *IEEE J. Emerg. Sel. Topics Power Electron.*, vol. 2, no. 4, pp. 972–984, Dec. 2014.

[93] Y. He, X. Wang, X. Ruan, D. Pan, X. Xu, and F. Liu, "Capacitor-current proportional-integral positive feedback active damping for LCL-type grid-connected inverter to achieve high robustness against grid impedance variation," *IEEE Trans. Power Electron.*, to be published. doi: 10.1109/TPEL.2019.2906217.

[94] X. Wang, F. Blaabjerg, and P. C. Loh, "Virtual RC damping of LCL-filtered voltage source converters with extended selective harmonic compensation," *IEEE Trans. Power Electron.*, vol. 30, no. 9, pp. 4726–4737, Sep. 2015.

[95] J. Samanes, A. Urtasun, E. Gubia, and A. Petri, "Robust multisampled capacitor voltage active damping for grid-connected power converters," *Int. J. Electr. Power Energy Syst.*, vol. 105, pp. 741–752, Feb. 2019.

[96] M. Malinowski and S. Bernet, "A simple voltage sensorless active damping scheme for three-phase PWM converters with an *LCL* filter," *IEEE Trans. Ind. Electron.*, vol. 55, no. 4, pp. 1876–1880, Apr. 2008.

[97] A. Ghanem, M. Rashed, M. Sumner, M. A. Elsayes, and I. I. I. Mansy, "Hybrid active damping of LCL-filtered grid connected converter," in *Proc. IEEE Aunu. Southern Power Electron. Conf. (SPEC)*, Dec. 2016, pp. 1–6.

[98] R. Peña-Alzola, M. Liserre, F. Blaabjerg, R. Sebastián, J. Dannehl, and F. W. Fuchs, "Systematic design of the lead-lag network method for active damping in LCL-filter based three phase converters," *IEEE Trans. Ind. Informat.*, vol. 10, no. 1, pp. 43–52, Feb. 2014.
[99] Z. Xin, X. Wang, P. C. Loh, and F. Blaabjerg, "Digital realization of capacitor-voltage feedback active damping for LCL-filtered grid converters," in *Proc. IEEE Energy Convers. Congr. Expo. (ECCE)*, Spe. 2015, pp. 2690–2697.
[100] Z. Xin, P. C. Loh, X. Wang, F. Blaabjerg, and Y. Tang, "Highly accurate derivatives for LCL-filtered grid converter with capacitor voltage active damping," *IEEE Trans. Power Electron.*, vol. 31, no. 5, pp. 3612–3625, May 2016.
[101] C. Nie, Y. Wang, W. Lei, M. Chen, and Y. Zhang, "An enhanced control strategy for multiparalleled grid-connected single-phase converters with load harmonic current compensation capability," *IEEE Trans. Ind. Electron.*, vol. 65, no. 7, pp. 5623–5633, Jul. 2018.
[102] Y. Guan, Y. Wang, Y. Xie, Y. Liang, A. Lin, and X. Wang, "The dual-current control strategy of grid-connected inverter with *LCL* filter," *IEEE Trans. Power Electron.*, vol. 34, no. 6, pp. 5940–5952, Jun. 2019.
[103] J. W. He and Y. W. Li, "Generalized closed-loop control schemes with embedded virtual impedances for voltage source converters with LC or LCL filters," *IEEE Trans. Power Electron.*, vol. 27, no. 4, pp. 1850–1861, Apr. 2012.
[104] G. Shen, X. Zhu, J. Zhang, and D. Xu, "A new feedback method for PR current control of LCL-filter-based grid-connected inverter," *IEEE Trans. Ind. Electron.*, vol. 57, no. 6, pp. 2033–2041, Jun. 2010.
[105] N. He, D. Xu, Y. Zhu, J. Zhang, G. Shen, Y. Zhang, J. Ma, and C. Liu, "Weighted average current control in a three-phase grid inverter with an LCL filter," *IEEE Trans. Power Electron.*, vol. 28, no. 6, pp. 2785–2797, Jun. 2013.
[106] D. Pan, X. Ruan, X. Wang, H. Yu, and Z. Xing, "Analysis and design of current control schemes for LCL-type grid-connected inverter based on a general mathematical model," *IEEE Trans. Power Electron.*, vol. 32, no. 6, pp. 4395–4410, Jun. 2017.
[107] L. Zhou, X. Zhou, Y. Chen, Z. Lv, Z. He, W. Wu, L. Yang, K. Yan, A. Luo, and J. M. Guerrero, "Inverter-current-feedback resonance-suppression method for LCL-type DG system to reduce resonance-frequency offset and grid-inductance effect," *IEEE Trans. Ind. Electron.*, vol. 65, no. 9, pp. 7036–7048, Sep. 2018.
[108] J. Xu, S. Xie, and T. Tang, "Active damping-based control for grid-connected *LCL*-filtered inverter with injected grid current feedback only," *IEEE Trans. Ind. Electron.*, vol. 61, no. 9, pp. 4746–4758, Sep. 2014.
[109] X. Wang, F. Blaabjerg, and P. C. Loh, "Grid-current-feedback active damping for LCL resonance in grid-connected voltage-source converters," *IEEE Trans. Power Electron.*, vol. 31, no. 1, pp. 213–223, Jan. 2016.
[110] Z. Lin, W. Yao, Z. Bai, and Z. Lu, "Study on active damping of LCL filter resonance based on grid current feedback compensation," in *Proc. IEEE Int. Symp. Ind. Electron. (ISIE)*, May 2013, pp. 1–6.
[111] M. Hanif, V. Khadkikar, W. Xiao, and J. L. Kirtley, "Two degrees of freedom active damping technique for LCL filter-based grid connected PV systems," *IEEE Trans. Ind. Electron.*, vol. 61, no. 6, pp. 2795–2803, Jun. 2014.
[112] R. A. Fantino, C. A. Busada, and J. A. Solsona, "Optimum PR control applied to *LCL* filters with low resonance frequency," *IEEE Trans. Power Electron.*, vol. 33, no. 1, pp. 793–801, Jan. 2018.
[113] Y. Chen, Z. Xie, L. Zhou, Z. Wang, X. Zhou, W. Wu, L. Yang, and A. Luo, "Optimized design method for grid-current-feedback active damping to improve dynamic characteristic of LCL-type grid-connected inverter," *Int. J. Electr. Power Energy Syst.*, vol. 100, pp. 19–28, Sep. 2018.
[114] X. P. Zhou, L. Zhou, Y. Chen, Z. Shuai, J. M. Guerrero, A. Luo, W. Wu, and L. Yang, "Robust grid-current-feedback resonance suppression method for LCL-type grid-connected inverter connected to weak grid," *IEEE J. Emerg. Sel. Topics Power Electron.*, vol. 6, no. 4, pp. 2126–2137, Dec. 2018.
[115] Z. Xin, X. Wang, P. C. Loh, and F. Blaabjerg, "Grid-current-feedback control for LCL-filtered grid converters with enhanced stability," *IEEE Trans. Power Electron.*, vol. 32, no. 4, pp. 3216–3228, Apr. 2017.
[116] J. Wang, J. D. Yan, and J. Zou, "Inherent damping of single-loop digitally controlled voltage source inverters with *LCL* filters," in *Proc. IEEE Int. Symp. Ind. Electron. (ISIE)* , Jun. 2016, pp. 487–492.
[117] X. Zhang, J. W. Spencer, and J. M. Guerrero, "Small-signal modeling of digitally controlled grid-connected inverters with LCL filters," *IEEE Trans. Ind. Electron.*, vol. 60, no. 9, pp. 3752–3765, Sep. 2013.
[118] D. G. Holmes, T. A. Lipo, B. P. McGrath, and W. Y. Kong, "Optimized design of stationary frame three phase AC current regulators," *IEEE Trans. Power Electron.*, vol. 24, no. 11, pp. 2417–2426, Nov. 2009.
[119] C. Zou, B. Liu, S. Duan, and R. Li, "Influence of delay on system stability and delay optimization of grid-connected inverters with LCL filter," *IEEE Trans. Ind. Informat.*, vol. 10, no. 3, pp. 1775–1784, Aug. 2014.
[120] D. Yang, X. Ruan, and H. Wu, "A real-time computation method with dual sampling mode to improve the current control performance of the LCL-type grid-connected inverter," *IEEE Trans. Ind. Electron.*, vol. 62, no. 7, pp. 4563–4572, Jul. 2015.
[121] Y. Tang, P. C. Loh, P. Wang, F. H. Choo, and F. Gao, "Exploring inherent damping characteristic of *LCL*-filters for three-phase grid-connected voltage source inverters," *IEEE Trans. Power Electron.*, vol. 27, no. 3, pp. 1433–1443, Mar. 2012.
[122] J. Yin, S. Duan, and B. Liu, "Stability analysis of grid-connected inverter with LCL filter adopting a digital single-loop controller with inherent damping characteristic," *IEEE Trans. Ind. Informat.*, vol. 9, no. 2, pp. 1104–1112, May 2013.
[123] A. Kahrobaeian and Y. A.-R. I. Mohamed, "Robust single-loop direct current control of *LCL*-filtered converter-based DG units in grid-connected and autonomous microgrid modes," *IEEE Trans. Power Electron.*, vol. 29, no. 10, pp. 5605–5619, Oct. 2014.
[124] S. G. Parker, B. P. McGrath, and D. G. Holmes, "Regions of active damping control for *LCL* filters," *IEEE Trans. Ind. Appl.*, vol. 50, no. 1, pp. 424–432, Jan./Feb. 2014.
[125] J. Wang, J. Yan, L. Jiang, and J. Zou, "Delay-dependent stability of single-loop controlled grid-connected inverters with *LCL* filters," *IEEE Trans. Power Electron.*, vol. 31, no. 1, pp. 743–757, Jan. 2016.
[126] X. Li, X. Wu, Y. Geng, X. Yuan, C. Xia, and X. Zhang, "Wide damping region for LCL-type grid-connected inverter with an improved capacitor-current-feedback method," *IEEE Trans. Power Electron.*, vol. 30, no. 9, pp. 5247–5259, Sep. 2015.
[127] T. Nussbaumer, M. L. Heldwein, G. Gong, S. D. Round, and J. W. Kolar, "Comparison of prediction techniques to compensate time delays caused by digital control of a three-phase buck-type PWM rectifier system," *IEEE Trans. Ind. Electron.*, vol. 55, no. 2, pp. 791–799, Feb. 2008.
[128] F. de Bosio, L. A. de S. Ribeiro, F. D. Freijedo, M. Pastorelli, and J. M. Guerrero, "Discrete-time domain modeling of voltage source inverters in standalone applications: Enhancement of regulators performance by means of Smith predictor," *IEEE Trans. Power Electron.*, vol. 32, no. 10, pp. 8100–8114, Oct. 2017.
[129] V. Miskovic, V. Blasko, T. M. Jahns, A. H. C. Smith, and C. Romenesko, "Observer-based active damping of *LCL* resonance in grid-connected voltage source converters," *IEEE Trans. Ind. Appl.*, vol. 50, no. 6, pp. 3977–3985, Nov./Dec. 2014.
[130] M. G. Judewicz, S. A. González, J. R. Fischer, J. F. Martínez, and D. O. Carrica, "Inverter-side current control of grid-connected voltage source inverters with LCL filter based on generalized predictive control," *IEEE J. Emerg. Sel. Topics Power Electron.*, vol. 6, no. 4, pp. 1732–1743, Dec. 2018.
[131] S. Bibian and H. Jin, "Time delay compensation of digital control for DC switchmode power supplies using prediction techniques," *IEEE Trans. Power Electron.*, vol. 15, no. 5, pp. 835–842, Sep. 2000.
[132] B. Cao, L. Chang, and R. Shao, "Predictive current controller for single-phase grid-connected VSIs with compensation for time-delay effect and system uncertainty," *IEEE J. Emerg. Sel. Topics Power Electron.*, vol. 6, no. 4, pp. 1761–1768, Dec. 2018.
[133] M. Semasa, T. Kato, and K. Inoue, "A simple and effective time delay compensation method for grid-connected inverter with an LCL filter: Application to active damping method," in *Proc. IEEE Workshop Control Model. Power Electron. (COMPEL)*, Jul. 2017, pp. 1–7.
[134] C. Chen, J. Xiong, Z. Wan, J. Lei, and K. Zhang, "A time delay compensation method based on area equivalence for active damping of an LCL-type converter," *IEEE Trans. Power Electron.*, vol. 32, no. 1, pp. 762–772, Jan. 2017.
[135] T. Liu, Z. Liu, J. Liu, Y. Tu, and Z. Liu, "An improved capacitor-current-feedback active damping for LCL resonance in grid-connected inverters," in *Proc. IEEE Int. Future Energy Electron. Conf. ECCE Asia (IFEEC-ECCE Asia)*, Jun. 2017, pp. 2111–2116.
[136] Y. He, X. Wang, and X. Ruan, "Improve the robustness of digitally-controlled LCL-filtered inverters against grid impedance variation with a lag compensator," in *Proc. IEEE Energy Convers. Congr. Expo. (ECCE)*, Oct. 2017, pp. 76–82.

[137] D. Pan, X. Ruan, C. Bao, W. Li, and X. Wang, "Optimized controller design for LCL-type grid-connected inverter to achieve high robustness against grid-impedance variation," *IEEE Trans. Ind. Electron.*, vol. 62, no. 3, pp. 1537–1547, Mar. 2015.

[138] T. Liu, Z. Liu, J. Liu, Y. Tu, and Z. Liu, "Stability enhancement of single-loop inverter-side current feedback controlled grid-connected inverters with *LCL* filters," in *Proc. IEEE Energy Convers. Congr. Expo. (ECCE)*, Oct. 2017, pp. 3030–3037.

[139] Q. Huang and K. Rajashekara, "Virtual RLC active damping for grid-connected inverters with LCL filters," in *Proc. IEEE Appl. Power Electron. Conf. Expo. (APEC)*, Mar. 2017, pp. 424–429.

[140] H. Liu, L. Li, X. Zheng, Z. Xu, D. Xu, and Q. Gao, "An improved active damping control in grid-connected converter system," in *Proc. IEEE Ind. Electron. Soc. Annu. Conf. (IECON)*, Oct./Nov. 2017, pp. 2396–2401.

[141] M. Lu, X. Wang, P. C. Loh, F. Blaabjerg, and T. Dragicevic, "Graphical evaluation of time-delay compensation techniques for digitally controlled converters," *IEEE Trans. Power Electron.*, vol. 33, no. 3, pp. 2601–2614, Mar. 2018.

[142] J. Liu, L. Zhou, B. Li, C. Zheng, and B. Xie, "Modeling and analysis of a digitally controlled grid-connected large-scale centralized PV system," *IEEE Trans. Power Electron.*, vol. 33, no. 5, pp. 4000–4014, May 2018.

[143] J. Liu, L. Zhou, and M. Molinas, "Damping region extension for digitally controlled LCL-type grid-connected inverter with capacitor-current feedback," *IET Power Electron.*, vol. 11, no. 12, pp. 1974–1982, Oct. 2018.

[144] L. Yang and J. Yang, "A robust dual-loop current control method with a delay-compensation control link for *LCL*-type shunt active power filters," *IEEE Trans. Power Electron.*, vol. 34, no. 7, pp. 6183–6199, Jul. 2019.

[145] L. Corradini, W. Stefanutti, and P. Mattavelli, "Analysis of multisampled current control for active filters," *IEEE Trans. Ind. Appl.*, vol. 44, no. 6, pp. 1785–1794, Nov. 2008.

[146] X. Zhang, P. Chen, C. Yu, F. Li, H. T. Do, and R. Cao, "Study of a current control strategy based on multisampling for high-power grid-connected inverters with an LCL filter," *IEEE Trans. Power Electron.*, vol. 32, no. 7, pp. 5023–5034, Jul. 2017.

[147] X. Zhang and J. W. Spencer, "Study of multisampled multilevel inverters to improve control performance," *IEEE Trans. Power Electron.*, vol. 27, no. 11, pp. 4409–4416, Nov. 2012.

[148] Z. Wan, J. Xiong, J. Lei, and C. Chen, "Analyze and reduce the impact of sampling delay on LCL converter with capacitor current feedback active damping," in *Proc. IEEE Int. Conf. Power Electron. Drive Syst. (PEDS)*, Jun. 2015, pp. 539–545.

[149] X. Li, J. Fang, Y. Tang, X. Wu, and Y. Geng, "Capacitor-voltage feedforward with full delay compensation to improve weak grids adaptability of *LCL*-filtered grid-connected converters for distributed generation systems," *IEEE Trans. Power Electron.*, vol. 33, no. 1, pp. 749–764, Jan. 2018.

[150] R. D. Middlebrook, "Input filter considerations in design and application of switching regulators," in *Proc. IEEE Ind. Appl. Soc. Annu. Meeting*, Jan. 1976, pp. 366–382.

[151] X. Chen, Y. Zhang, S. Wang, J. Chen, and C. Gong, "Impedance-phased dynamic control method for grid-connected inverters in a weak grid," *IEEE Trans. Power Electron.*, vol. 32, no. 1, pp. 274–283, Jan. 2017.

[152] Y. He, H. S.-H. Chung, C.-T. Lai, X. Zhang, and W. Wu, "Active cancelation of equivalent grid impedance for improving stability and injected power quality of grid-connected inverter under variable grid condition," *IEEE Trans. Power Electron.*, vol. 33, no. 11, pp. 9387–9398, Nov. 2018.

[153] D. Yang, X. Ruan, and H. Wu, "Impedance shaping of the grid-connected inverter with LCL filter to improve its adaptability to the weak grid condition," *IEEE Trans. Power Electron.*, vol. 29, no. 11, pp. 5795–5805, Nov. 2014.

[154] Y. Han, M. Luo, X. Zhao, J. M. Guerrero, and L. Xu, "Comparative performance evaluation of orthogonal-signal-generators-based single-phase PLL algorithms—A survey," *IEEE Trans. Power Electron.*, vol. 31, no. 5, pp. 3932–3944, May 2016.

[155] L. Jia, X. Ruan, W. Zhao, Z. Lin, and X. Wang, "An adaptive active damper for improving the stability of grid-connected inverters under weak grid," *IEEE Trans. Power Electron.*, vol. 33, no. 11, pp. 9561–9574, Nov. 2018.

[156] Z. Lin, Z. Chen, L. Yajuan, L. Bin, L. Jinhong, and X. Bao, "Phase-reshaping strategy for enhancing grid-connected inverter robustness to grid impedance," *IET Power Electron.*, vol. 11, no. 8, pp. 1434–1443, Jul. 2018.

[157] J. Xu, S. Xie, B. Zhang, and Q. Qian, "Robust grid current control with impedance-phase shaping for *LCL*-filtered inverters in weak and distorted grid," *IEEE Trans. Power Electron.*, vol. 33, no. 12, pp. 10240–10250, Dec. 2018.

[158] A. Akhavan, H. R. Mohammadi, and J. M. Guerrero, "A comprehensive control system for multi-parallel grid-connected inverters with *LCL* filter in weak grid condition," *Electric Power Syst. Res.*, vol. 163, pp. 288–300, Oct. 2018.

[159] B. Wen, R. Burgos, D. Boroyevich, P. Mattavelli, and Z. Shen, "AC stability analysis and DQ frame impedance specifications in power-electronics-based distributed power systems," *IEEE J. Emerg. Sel. Topics Power Electron.*, vol. 5, no. 4, pp. 1455–1465, Dec. 2017.

[160] S. Zhou, X. Zou, D. Zhu, L. Tong, Y. Zhao, Y. Kang, and X. Yuan, "An improved design of current controller for LCL-type grid-connected converter to reduce negative effect of PLL in weak grid," *IEEE J. Emerg. Sel. Topics Power Electron.*, vol. 6, no. 2, pp. 648–663, Jun. 2018.

[161] B. Wen, D. Boroyevich, P. Mattavelli, Z. Shen, and R. Burgos, "Influence of phase-locked loop on input admittance of three-phase voltage-source converters," in *Proc. IEEE Appl. Power Electron. Conf. Expo. (APEC)*, Mar. 2013, pp. 897–904.

[162] B. Wen, D. Boroyevich, P. Mattavelli, R. Burgos, and Z. Shen, "Modeling the output impedance negative incremental resistance behavior of grid-tied inverters," in *Proc. IEEE Appl. Power Electron. Conf. Expo. (APEC)*, Mar. 2014, pp. 1799–1806.

[163] B. Wen, D. Boroyevich, R. Burgos, P. Mattavelli, and Z. Shen, "Analysis of D-Q small-signal impedance of grid-tied inverters," *IEEE Trans. Power Electron.*, vol. 31, no. 1, pp. 675–687, Jan. 2016.

[164] B. Wen, D. Dong, D. Boroyevich, P. Mattavelli, R. Burgos, and Z. Shen, "Impedance-based analysis of grid-synchronization stability for three-phase paralleled converters," *IEEE Trans. Power Electron.*, vol. 31, no. 1, pp. 26–38, Jan. 2016.

[165] Y. Liao, Z. Liu, H. Zhang, and B. Wen, "Low-frequency stability analysis of single-phase system with *dq*-frame impedance approach—Part I: Impedance modeling and verification," *IEEE Trans. Ind. Appl.*, vol. 54, no. 5, pp. 4999–5011, Sep./Oct. 2018.

[166] X. Zhang, D. Xia, Z. Fu, G. Wang, and D. Xu, "An improved feedforward control method considering PLL dynamics to improve weak grid stability of grid-connected inverters," *IEEE Trans. Ind. Appl.*, vol. 54, no. 5, pp. 5143–5151, Sep./Oct. 2018.

[167] J. Fang, X. Li, H. Li, and Y. Tang, "Stability improvement for three-phase grid-connected converters through impedance reshaping in quadrature-axis," *IEEE Trans. Power Electron.*, vol. 33, no. 10, pp. 8365–8375, Oct. 2018.

[168] Y. Tang, J. Fang, X. Li, and H. Li, "Reshaping quadrature-axis impedance of three-phase grid-connected converters for low-frequency stability improvement," in *Proc. Int. Power Electron. Conf. (IPEC-ECCE Asia)*, May 2018, pp. 3910–3915.

[169] B. Wen, D. Boroyevich, R. Burgos, P. Mattavelli, and Z. Shen, "Small-signal stability analysis of three-phase AC systems in the presence of constant power loads based on measured d-q frame impedances," *IEEE Trans. Power Electron.*, vol. 30, no. 10, pp. 5952–5963, Oct. 2015.

[170] G. Francis, R. Burgos, D. Boroyevich, F. Wang, and K. Karimi, "An algorithm and implementation system for measuring impedance in the D-Q domain," in *Proc. IEEE Energy Convers. Congr. Expo. (ECCE)*, Sep. 2011, pp. 3221–3228.

[171] S. Lissandron, L. D. Santa, P. Mattavelli, and B. Wen, "Experimental validation for impedance-based small-signal stability analysis of single-phase interconnected power systems with grid-feeding inverters," *IEEE J. Emerg. Sel. Topics Power Electron.*, vol. 4, no. 1, pp. 103–115, Mar. 2016.

[172] S. Shah and L. Parsa, "Impedance modeling of three-phase voltage source converters in DQ, sequence, and phasor domains," *IEEE Trans. Energy Convers.*, vol. 32, no. 3, pp. 1139–1150, Sep. 2017.

[173] M. Céspedes and J. Sun, "Methods for stability analysis of unbalanced three-phase systems," in *Proc. IEEE Energy Convers. Congr. Expo. (ECCE)*, Sep. 2012, pp. 3090–3097.

[174] M. Cespedes and J. Sun, "Impedance modeling and analysis of grid-connected voltage-source converters," *IEEE Trans. Power Electron.*, vol. 29, no. 3, pp. 1254–1261, Mar. 2014.

[175] M. K. Bakhshizadeh, X. Wang, F. Blaabjerg, J. Hjerrild, Ł. Kocewiak, C. L. Bak, and B. Hesselbæk, "Couplings in phase domain impedance modeling of grid-connected converters," *IEEE Trans. Power Electron*, vol. 31, no. 10, pp. 6792–6796, Oct. 2016.

[176] A. Rygg, M. Molinas, C. Zhang, and X. Cai, "A modified sequence-domain impedance definition and its equivalence to the dq-domain impedance definition for the stability analysis of AC power electronic systems," *IEEE J. Emerg. Select. Topics Power Electron.*, vol. 4, no. 4, pp. 1383–1396, Dec. 2016.
[177] H. Nian, L. Chen, Y. Xu, H. Huang, and J. Ma, "Sequences domain impedance modeling of three-phase grid-connected converter using harmonic transfer matrices," *IEEE Trans. Energy Convers.*, vol. 33, no. 2, pp. 627–638, Jun. 2018.
[178] A. Rygg, M. Molinas, C. Zhang, and X. Cai, "On the equivalence and impact on stability of impedance modeling of power electronic converters in different domains," *IEEE J. Emerg. Sel. Topics Power Electron.*, vol. 5, no. 4, pp. 1444–1454, Dec. 2017.
[179] C. Zhang, X. Cai, A. Rygg, and M. Molinas, "Sequence domain SISO equivalent models of a grid-tied voltage source converter system for small-signal stability analysis," *IEEE Trans. Energy Convers.*, vol. 33, no. 2, pp. 741–749, Jun. 2018.
[180] A. G. J. MacFarlane and I. Postlethwaite, "The generalized Nyquist stability criterion and multivariable root loci," *Int. J. Control*, vol. 25, no. 1, pp. 81–127, 1977.
[181] M. Cespedes and J. Sun, "Adaptive control of grid-connected inverters based on online grid impedance measurements," *IEEE Trans. Sustainable Energy*, vol. 5, no. 2, pp. 516–523, Apr. 2014.
[182] P. García, M. Sumner, Á. Navarro-Rodríguez, J. M. Guerrero, and J. García, "Observer-based pulsed signal injection for grid impedance estimation in three-phase systems," *IEEE Trans. Ind. Electron.*, vol. 65, no. 10, pp. 7888–7899, Oct. 2018.
[183] R. Luhtala, T. Messo, T. Reinikka, J. Sihvo, T. Roinila, and M. Vilkko, "Adaptive control of grid-connected inverters based on real-time measurements of grid impedance: DQ-domain approach," in *Proc. IEEE Energy Convers. Congr. Expo. (ECCE)*, Oct. 2017, pp. 69–75.
[184] R. Luhtala, T. Messo, and T. Roinila, "Adaptive control of grid-voltage feedforward for grid-connected inverters based on real-time identification of grid impedance," in *Proc. Int. Power Electron. Conf. (IPEC-ECCE Asia)*, May 2018, pp. 547–554.
[185] T. Roinila, M. Vilkko, and J. Sun, "Online grid impedance measurement using discrete-interval binary sequence injection," in *Proc. IEEE 14th Workshop Control Model. Power Electron. (COMPEL)*, Jun. 2013, pp. 1–8.
[186] T. Roinila, M. Vilkko, and J. Sun, "Online grid impedance measurement using discrete-interval binary sequence injection," *IEEE J. Emerg. Sel. Topics Power Electron.*, vol. 2, no. 4, pp. 985–993, Dec. 2014.
[187] T. Roinila, T. Messo, and A. Aapro, "Impedance measurement of three phase systems in DQ-domain: Applying MIMO-identification techniques," in *Proc. IEEE Energy Convers. Congr. Expo. (ECCE)*, Sep. 2016, pp. 1–6.
[188] R. Luhtala, T. Roinila, and T. Messo, "Implementation of real-time impedance-based stability assessment of grid-connected systems using MIMO-identification techniques," *IEEE Trans. Ind. Appl.*, vol. 54, no. 5, pp. 5054–5063, Sep./Oct. 2018.
[189] T. Roinila, T. Messo, and E. Santi, "MIMO-identification techniques for rapid impedance-based stability assessment of three-phase systems in DQ domain," *IEEE Trans. Power Electron.*, vol. 33, no. 5, pp. 4015–4022, May 2018.
[190] T. Roinila and T. Messo, "Online grid-impedance measurement using ternary-sequence injection," *IEEE Trans. Ind. Appl.*, vol. 54, no. 5, pp. 5097–5103, Sep./Oct. 2018.
[191] A. Knop and F. W. Fuchs, "High frequency grid impedance analysis by current injection," in *Proc. IEEE Ind. Electron. Annu. Conf. (IECON)*, Nov. 2009, pp. 536–541.
[192] T. Messo, R. Luhtala, T. Roinila, D. Yang, X. Wang, and F. Blaabjerg, "Real-time impedance-based stability assessment of grid converter interactions," in *Proc. IEEE 18th Workshop Control Modeling Power Electron. (COMPEL)*, Jul. 2017, pp. 1–8.
[193] Z. Chen, A. Luo, Y. Chen, and M. Li, "Resonance features of multi-paralleled grid-connected inverters and its damping method," in *Proc. Int. Power Electron. Appl. Conf. Expo. (PEAC)*, Nov. 2014, pp. 120–125.
[194] M. Lu, X. Wang, P. C. Loh, and F. Blaabjerg, "Resonance interaction of multiparallel grid-connected inverters with LCL filter," *IEEE Trans. Power Electron.*, vol. 32, no. 2, pp. 894–899, Feb. 2017.
[195] M. Lu, Y. Yang, B. Johnson, and F. Blaabjerg, "An interaction-admittance model for multi-inverter grid-connected systems," *IEEE Trans. Power Electron.*, vol. 34, no. 8, pp. 7542–7557, Aug. 2019.
[196] Q. Qian, S. Xie, L. Huang, J. Xu, Z. Zhang, and B. Zhang, "Harmonic suppression and stability enhancement for parallel multiple grid-connected inverters based on passive inverter output impedance," *IEEE Trans. Ind. Electron.*, vol. 64, no. 9, pp. 7587–7598, Sep. 2017.
[197] F. Cavazzana, T. Caldognetto, P. Mattavelli, M. Corradin, and I. Toigo, "Analysis of current control interaction of multiple parallel grid-connected inverters," *IEEE Trans. Sustain. Energy*, vol. 9, no. 4, pp. 1740–1749, Oct. 2018.
[198] C. Zheng, Q. Li, L. Zhou, B. Li, and M. Mao, "The interaction stability analysis of a multi-inverter system containing different types of inverters," *Energies*, vol. 11, no. 9, p. 2244, Aug. 2018.
[199] X. Wang, F. Blaabjerg, and W. Wu, "Modeling and analysis of harmonic stability in an AC power-electronics-based power system," *IEEE Trans. Power Electron.*, vol. 29, no. 12, pp. 6421–6432, Dec. 2014.
[200] X. Zhang, H. S.-H. Chung, L. L. Cao, J. P. W. Chow, and W. Wu, "Impedance-based stability criterion for multiple offshore inverters connected in parallel with long cables," in *Proc. IEEE Energy Convers. Congr. Expo. (ECCE)*, Oct. 2017, pp. 3383–3389.
[201] T. Chen, C.-K. Lee, and S. Y. R. Hui, "A general design procedure for multi-parallel modular grid-tied inverters system to prevent common and interactive instability," *IEEE Trans. Power Electron.*, vol. 34, no. 7, pp. 6025–6030, Jul. 2019.
[202] X. Wang, F. Blaabjerg, M. Liserre, Z. Chen, J. He, and Y. Li, "An active damper for stabilizing power-electronics-based AC systems," *IEEE Trans. Power Electron.*, vol. 29, no. 7, pp. 3318–3329, Jul. 2014.

YANG HAN (S'08–M'10–SM'17) received the Ph.D. degree in electrical engineering from Shanghai Jiao Tong University (SJTU), Shanghai, China, in 2010.

In 2010, he joined the Department of Power Electronics, School of Mechatronics Engineering, University of Electronic Science and Technology of China (UESTC), Chengdu, China, where he has been an Associate Professor, since 2013. From March 2014 to March 2015, he was a Visiting Scholar with the Department of Energy Technology, Aalborg University, Aalborg, Denmark. He is currently with the Department of Electrical Engineering, School of Mechanical and Electrical Engineering, UESTC. He has authored more than 20 ISI-indexed international journal papers, including three ESI highly cited papers, one ESI hot paper, and one book chapter in the area of power electronics, power quality conditioners, and smart grid. He holds 25 issued and nine pending patents. His research interests include the ac/dc microgrids, active distribution networks, power quality, grid-connected converters for renewable energy systems, active power filters, multilevel converters, and static synchronous compensators (STATCOMs).

Dr. Han was the recipient of the Academic Talent Award by UESTC, in 2017, Baekhyun Award by the Korean Institute of Power Electronics, in 2016, the Best Paper Awards from the 34th Annual Conference on Power System and Automation of Chinese Universities, in 2018, the Joint Conference of Sichuan Power Supply Society and Chongqing Power Supply Society, in 2018, the 6th Asia International Symposium on Mechatronics, in 2017, the 5th National Conference on Power Quality, in 2017, the Annual Conference of HVDC and Power Electronics Committee of Chinese Society of Electrical Engineers, in 2013, and the 4th International Conference on Power Quality, in 2008, China. He was a Session Chair for Emerging Technologies and End-User Systems, Grid Operation and Management, and Power Electronics, Control and Protection Systems for Smart Grids Sessions in the IEEE PES Innovative Smart Grid Technologies Asia (ISGT Asia 2019), Chengdu, China, in 2019, for Microgrid and Distributed Generation Session in the Symposium on Power Electronics and Electrical Drives (SPEED), Xi'an, China, in 2019, for Microgrid Optimization and Scheduling Session in the 2nd International Conference on Power and Renewable Energy, Chengdu, China, in 2017, for Power Quality Mitigation and Application Session in the 5th National Conference on Power Quality, Xi'an, in 2017, and for AC/DC, DC/AC Power Converter Session in the 2016 IPEMC ECCE-Asia, Hefei, China. He is an Associate Editor for IEEE Access and the *Journal of Power Electronics* (JPE).

MENGLING YANG received the B.S. degree in electrical engineering and automation from Sichuan Normal University, Chengdu, China, in 2018. He is currently pursuing the M.S. degree in power electronics and electric drives with the University of Electronic Science and Technology of China (UESTC), Chengdu, China. His current research interests include the modeling, control, and stability analysis of inverters.

HONG LI received the B.S. degree in electrical engineering and automation and the M.S. degree in power electronics and electric drives from the University of Electronic Science and Technology of China (UESTC), Chengdu, China, in 2015 and 2018, respectively. Since 2018, he has been with the Chengdu Aircraft Industrial Corporation, Chengdu. His current research interests include the optimization of ac microgrids, power management, hierarchical and cooperative control, and the grid-integration of renewable energy resources.

PING YANG received the B.S. degree from Shanghai Jiao Tong University (SJTU), Shanghai, China, in 1984, and the M.S. degree from Sichuan University, in 1987, both in mechanical engineering. He held a visiting position at Victory University, Australia, from July 2004 to August 2004, a Visiting Scholar with the S. M. Wu Manufacturing Research Center, University of Michigan, Ann Arbor, USA, from August 2009 to February 2010, and held a visiting position at the University of California at Irvine, Irvine, USA, from October 2012 to November 2012. He is currently a Full Professor with the School of Mechatronics Engineering, University of Electronic Science and Technology of China (UESTC), Chengdu, China, and the Dean of the School of Mechanical and Electrical Engineering, UESTC.

He has authored more than 60 papers in various journals and international conferences, and several books on mechatronics and instrumentation. His research interests include mechatronics engineering, electrical engineering and automation, computer-aided control and instrumentation, smart mechatronics, and detection and automation of mechanical equipment. He received several provincial awards for his contribution in teaching and academic research.

LIN XU received the Ph.D. degree in electrical engineering from Shanghai Jiao Tong University (SJTU), Shanghai, China, in 2011. She is currently a Senior Engineering with the Sichuan Electric Power Research Institute, State Grid Sichuan Electric Power Company, Chengdu, China. She has coauthored more than 20 journals and conference papers in power electronics and power systems.

Her research interests include power quality, power system analysis and real-time digital simulator (RTDS), flexible AC transmission systems (FACTS), such as STATCOMs and power quality conditioners (DVRs and APFs). She is an Active Reviewer of the IEEE TRANSACTIONS ON INDUSTRIAL ELECTRONICS, the IEEE TRANSACTIONS ON POWER ELECTRONICS, and *Electric Power Components and Systems*.

ERNANE ANTÔNIO ALVES COELHO received the B.S. degree in electrical engineering from the Federal University of Minas Gerais, Belo Horizonte, Brazil, in 1987, the M.S. degree from the Federal University of Santa Catarina, Florianopolis, Brazil, in 1989, and the Ph.D. degree from the Federal University of Minas Gerais, in 2000. In 1989, he joined the Electrical Engineering Faculty, Universidade Federal de Uberlandia, where he is currently a Full Professor. His research interests include power-factor correction, PV and fuel cell systems, microgrid modeling, and digital control by microcontrollers and DSPs.

JOSEP M. GUERRERO (S'01–M'04–SM'08–FM'15) received the B.S. degree in telecommunications engineering, the M.S. degree in electronics engineering, and the Ph.D. degree in power electronics from the Technical University of Catalonia, Barcelona, in 1997, 2000, and 2003, respectively. Since 2011, he has been a Full Professor with the Department of Energy Technology, Aalborg University, Denmark, where he is responsible for the Microgrid Research Program. Since 2012, he has been a Guest Professor with the Chinese Academy of Science and the Nanjing University of Aeronautics and Astronautics; since 2014, he has been the Chair Professor with Shandong University; since 2015, he has been a Distinguished Guest Professor with Hunan University; and since 2016, he has been a Visiting Professor Fellow with Aston University, U.K. His research interests oriented to different microgrid aspects, including power electronics, distributed energy-storage systems, hierarchical and cooperative control, energy management systems, smart metering and the Internet of Things for AC/DC microgrid clusters and islanded minigrids; current research specially focused on maritime microgrids for electrical ships, vessels, ferries, and seaports.

In 2015, he was elevated as the IEEE Fellow for his contributions on "distributed power systems and microgrids." He received the Best Paper Award of the IEEE TRANSACTIONS ON ENERGY CONVERSION from 2014 to 2015. In 2014 and 2015, he received a Thomson Reuters as Highly Cited Researcher. He was the Chair of the Renewable Energy Systems Technical Committee of the IEEE Industrial Electronics Society. He is an Associate Editor of the IEEE TRANSACTIONS ON POWER ELECTRONICS, the IEEE TRANSACTIONS ON INDUSTRIAL ELECTRONICS, and the *IEEE Industrial Electronics Magazine*, and an Editor of the IEEE TRANSACTIONS ON SMART GRID and the IEEE TRANSACTIONS ON ENERGY CONVERSION. He has been a Guest Editor of the IEEE TRANSACTIONS ON POWER ELECTRONICS Special Issues: Power Electronics for Wind Energy Conversion and Power Electronics for Microgrids; the IEEE TRANSACTIONS ON INDUSTRIAL ELECTRONICS Special Sections: Uninterruptible Power Supplies Systems, Renewable Energy Systems, Distributed Generation and Microgrids, and Industrial Applications and Implementation Issues of the Kalman Filter; the IEEE TRANSACTIONS ON SMART GRID Special Issues: Smart DC Distribution Systems and Power Quality in Smart Grids; the IEEE TRANSACTIONS ON ENERGY CONVERSION Special Issue on Energy Conversion in Next-Generation Electric Ships.